Comments to the editor:

- **The recommendation is that you avoid the term "Dead Sea drying out" entirely.**

The term "Dead Sea drying out" has been removed entirely in all places where it could lead to a misunderstanding.

Specifically, I suggest the following changes prior to accepting your paper for publication in ACP:

1) Change the title to emphasise the idealized aspects of your study. One option might be: "An idealized model sensitivity study on Dead Sea desertification with a focus on the impact on convection"

Thank you for the suggestion, the title has been changed using your suggestion which I consider very well represent the purpose of the paper clarifying the idealized-model representation of the Dead Sea in our simulations.

2) Change key words
Changed

3) Change abstract (lines 5, 14 where you mention "drying out of Dead Sea" - reword these sentences and better emphasise the idealized aspect of your sensitivity experiment.
Changes have been applied to the abstract following your suggestions. Instead of "drying out of Dead Sea" the concept of "changed conditions at the Dead Sea" has been used thought the paper and the idealized aspect of the sensitivity experiment in relation to the description of the Dead Sea characteristics has been explicitly exposed.

4) Abstract line 21: this last sentence is very vague. It would be good to give here more quantitative information about how much evaporation and precipitation decrease, and air temperature increases (the same again on line 560). If I interpret Fig. 2a correctly, then the effect on precipitation is very weak.
As you correctly mention the effect is very weak, as indicated previously in the manuscript about 0.5 %. This information has been included in the abstract and conclusions.

5) Please reconsider / clarify figure captions. For instance, Fig. 2 mentions "areal-daily averaged ... evaporation ..." and Fig. 4 mentions "monthly-daily accumulated areal mean values of evaporation ...". I don't understand "monthly-daily"?? I think that Fig. 2 shows area-averaged daily accumulated values and Fig. 4 shows area-averaged monthly accumulated values. Please clarify.
This information has been changed following the editor´s suggestion.

6) Change conclusions and general wording of simulations: emphasise idealized setup in line

554; and change several statements in lines 558ff. You could maybe refer to the "drying of the Dead Sea" sensitivity experiment in the entire paper as the "bare soil everywhere simulation" or shorter "bare soil simulation" and the control run as the "Dead Sea simulation".

This information has been modified throughout the paper following the editor´s suggestion.

7) line 562: I don't understand how a cooling effect can lead to an increase of temperature?? Please rephrase this sentence.

This sentence has been removed from this part of the text to avoid repetition since it has been described before in section 3.1.

8) line 621: careful - I am not sure that your study tells much about the effect of "lake level decline". Lake level decline means that there is still water but at a lower level and with reduced surface area. But your idealized experiment is a complete bare soil experiment, which is something else than a decline of the lake level. It could be rewarding to do several intermediate experiments between today's conditions and bare soil only.

The term "lake level decline" has been removed from the manuscript everywhere where it could lead to misunderstanding to the reader.

In follow-up experiments in the region, with improved description of the Dead Sea characteristics among other improvements, we are performing intermediate experiments, which we expect to publish in following publications.

Near East Desertification: sensitivity of the local conditions leading to convection to the Dead Sea drying out

An idealized model sensitivity study on Dead Sea desertification with a focus on the impact on convection

Con formato: Fuente: (Predeterminado) Arial, Negrita

Samiro Khodayar[1,2] and Johannes Hoerner[2]

[1]Institute of Meteorology and Climate Research (IMK-TRO), Karlsruhe Institute of

Technology (KIT), Karlsruhe, Germany

[2]Mediterranean Centre for Environmental Studies (CEAM), Valencia, Spain

* Corresponding author. E-mail address: Khodayar_sam@gva.es (S. Khodayar)

Mediterranean Centre for Environmental Studies (CEAM),

Technological Park, Charles R. Darwin Street, 14 46980 - Paterna - Valencia - Spain

1 Abstract

2 The Dead Sea desertification-threatened region is affected by continual lake level
3 decline and occasional, but life-endangering flash-floods. Climate change has
4 aggravated such issues in the past decades. In this study, the impact on local
5 conditions leading to heavy precipitation of the ~~drying out~~changing conditions of the
6 Dead Sea is investigated. Idealized s~~S~~ensitivity simulations with the high-resolution
7 convection-permitting regional climate model COSMO-CLM and several numerical
8 weather prediction (NWP) runs on an event time scale are performed over the Dead
9 Sea area. The simulations are idealized in the sense of the Dead Sea model
10 representation not accurately representing the real conditions, but given by an external
11 date set. A reference ~~simulation~~or Dead Sea ~~covering~~simulation covering the 2003 to
12 2013 period and a twin sensitivity ~~experiment~~or bare soil simulation, in which the Dead
13 Sea is ~~dried out and~~ set to bare soil, are compared. NWP simulations focus on heavy
14 precipitation events exhibiting relevant differences between the ~~reference~~ Dead Sea
15 and the ~~sensitivity~~ bare soil decadal realization to assess the impact on the underlying
16 convection-related processes.

17 The ~~drying out~~changing in the conditions of the Dead Sea is seen to affect the
18 atmospheric conditions leading to convection in two ways: (a) the local decrease in
19 evaporation reduces moisture availability in the lower boundary layer locally and in the
20 neighbouring, directly affecting atmospheric stability. Weaker updrafts characterize the
21 drier and more stable atmosphere of the simulations where the Dead Sea has been
22 dried out. (b) Thermally driven wind system circulations and resulting
23 divergence/convergence fields are altered preventing in many occasions convection
24 initiation because of the omission of convergence lines. On a decadal scale, the
25 difference between the simulations suggests a weak decrease in evaporation, higher
26 air temperatures and less precipitation (less than 0.5 %).

27

28

29

30

31

32

Key Words: Dead Sea ~~drying~~desertification, climate change, convection, heavy
precipitation, boundary layer, wind systems, high-resolution modelling

1. Introduction

The Eastern Mediterranean and the Middle East is a sensitive climate change area (Smiatek et al. 2011). The anticipated warming in the 21st century combined with the general drying tendency, suggest important regional impacts of climate change, which should be investigated to assess and mitigate local effects on society and ecosystems. The Dead Sea basin is dominated by semi-arid and arid climates except by the north-western part that is governed by Mediterranean climate (Greenbaum et al. 2006). It is an ideal area to study climate variation in the Near East. It was already discussed by Ashbel (1939) the influence of the Dead Sea on the climate of its neighbouring regions. The change in the climate of the Dead Sea basin caused by the drying of the Dead Sea has also been evidenced in the last decades (Alpert et al. 1997; Cohen and Stanhill 1996; Stanhill 1994). The Dead Sea is the lowest body of water in the world (~ -430 m) surrounded by the Judean Mountains (up to ~ 1 km amsl) to the west and to the east by the Maob Mountains (up to ~ 3 km amsl). The area in between is rocky desert. The complex topography of the area favours the combined occurrence of several wind regimes in addition to the general synoptic systems, namely valley and slope winds, Mediterranean breezes and local lake breezes (e.g. Shafir and Alpert 2011). These wind systems are of great importance for the living conditions in the region since they influence the visibility and the air quality (e.g. Kalthoff et al. 2000; Corsmeier et al. 2005) as well as the atmospheric temperature and humidity. Since the Dead Sea is a terminal lake of the Dead Sea Valley, no natural outflow exists; evaporation is the main loss of water. The wind velocity and vapour pressure deficit are identified as the main governing factors of evaporation throughout the year (Metzger et al. 2017). Through the high evaporation the lake level declines and results in a desertification of the shoreline and a changing fraction of water and land surface in the valley. The documented Dead Sea water level drop of about 1 m/y in the last decades (Gavrieli et al. 2005) is mainly due to the massive water consumption at its upstream having climate changes a small contribution to the lake level decrease (Lensky and Dente 2015). This situationseverely affects agriculture, industry and the environmental conditions in the area, thus, leading to substantial economic losses (Arkin and Gilat 2000).

67   The Jordan River catchment and Dead Sea exhibit in the north, annual precipitation in
68   the order of 600-800 mm, whereas in the south, there is an all year arid climate with an
69   annual precipitation of <150 mm (Schaedler and Sasse 2006). Rain occurs between
70   October and May and can be localized or widespread (Dayan and Sharon 1980)
71   (Sharon and Kutiel 1986). Rainfall varies seasonally and annually, and it is often
72   concentrated in intense showers (Greenbaum et al. 2006) caused mainly by severe
73   convection (Dayan and Morin 2006). Flash floods are among the most dangerous
74   meteorological hazards affecting the Mediterranean countries (Llasat et al 2010), thus,
75   knowledge about the processes shaping these events is of high value. This is
76   particularly relevant in arid climates, where rainfall is scarce, and often, local and highly
77   variable. In flood-producing rainstorms, atmospheric processes often act in concert at
78   several scales. Synoptic-scale processes transport and redistribute the excess sensible
79   and latent heat accumulated over the region and subsynoptic scale processes
80   determine initiation of severe convection and the resulting spatio-temporal rainfall
81   characteristics.   The main responsible synoptic weather patterns leading to heavy
82   rainfall in the region are in general well known and described in previous publications
83   (e.g. Belachsen et al. 2017; Dayan and Morin 2006). Belachsen et al. (2017) pointed
84   out that three main synoptic patterns are associated to these heavy rain events: Cyprus
85   low accounting for 30% of the events, Low to the east of the study region for 44%, and
86   Active Read Sea Trough for 26%. The first two originate from the Mediterranean Sea,
87   while the third is an extension of the Africa monsoon. Houze (2012) showed that
88   orographic effects lead to enhanced rainfall generation; rain cells are larger where
89   topography is higher. Sub-synoptic scale processes play a decisive role in deep
90   convection generation in the region. Convection generated by static instability seems to
91   play a more important role than synoptic-scale vertical motions (Dayan and Morin
92   2006). The moisture for developing intensive convection over the Dead Sea region can
93   be originated from the adjacent Mediterranean Sea (Alpert und Shay-EL 1994) and
94   from distant upwind sources (Dayan and Morin 2006).

95   In this study, the sensitivity of the local conditions in the Dead Sea region to the drying
96   outchanging conditions of the Dead Sea Sea is investigated focusing on the conditions
97   leading to heavy precipitating convection in the region. The relevance of the Dead Sea
98   as a local source of moisture for precipitating convection as well as the impact of the
99   energy balance partitioning changes and related processes caused by the drying of
100   thesetting the Dead Sea to bare soil are investigated. With this purpose, an idealized
101   sensitivity experiment with the high-resolution regional climate model COSMO-CLM
102   [Consortium for Small scale Modelling model (COSMO)-in Climate Mode (CLM); Böhm

103 et al. 2006] is conducted. The high horizontal grid spacing used (~ 2.8 km) resolves

104 relevant orographic and small-scale features of the Dead Sea basin, which is not the

105 case when coarser resolution simulations are performed. Moreover, at this resolution

106 convection is explicitly resolved instead of being parametrized, which has been already

107 extensively demonstrated to be highly beneficial for the simulation of heavy

108 precipitation and convection-related processes. The benefit of employing high-

109 resolution convection permitting simulations is mainly in sub-daily time-scales, (e.g.,

110 Prein et al., 2013; Fosser et al., 2014; Ban et al., 2014), however, daily precipitation is

111 also positively affected, particularly in winter time (Fosser et al., 2014). Previous

112 studies in the area applying high-resolution modelling agree with the beneficial impact

113 of finer resolution against coarser ones (e.g. Rostkier-~~Edelstein et~~Edelstein et al. 2014;

114 Hochman et al. 2018; Kunin et al. 2019).

115 A decadal simulation and several event-based Numerical Weather Prediction (NWP)

116 runs covering the eastern Mediterranean are carried out. A process understanding

117 methodology is applied to improve our knowledge about how sub-synoptic scale

118 processes leading to severe convection are affected ~~by the drying of the Dead Sea~~.

119 The article is organized as follows. Section 2 provides an overview of the data and the

120 methodology used. Then, in section 3, the climatology of the region based on the high-

121 resolution convection-permitting decadal simulation is presented and the impact of

122 ~~drying out~~changing conditions of the Dead Sea is examined across scales. Finally,

123 conclusions are discussed in section 4.

124

125 **2. Data and methodology**

126 **2.1 The COSMO-CLM model**

127 In this investigation, the regional climate model (RCM) of the non-hydrostatic COSMO

128 model, COSMO-CLM (CCLM), is used (Version 5.0.1). It has been developed by the

129 Consortium for Small-scale modeling (COSMO) and the Climate Limited-area Modeling

130 Community (CLM) (Böhm et al., 2006). It uses a rotated geographical grid and a

131 terrain-following vertical coordinate. The model domain covers the southern half of the

132 Levant, centred around the Dead Sea, with a horizontal resolution of 7 km and 2.8 km,

133 60 vertical levels and a time step of 60 and 20 seconds, respectively. Using IFS

134 (Integrated Forecasting System) analysis, the spectral weather model of ECMWF

135 (European Centre for Medium-Range Weather Forecast) as driving data for the

136 simulations, a double nesting procedure was employed. The coarsest nest at 0.0625º

137 resolution (about 7 km) covers 250 grid points in x direction and 250 grid points in y

138 direction. The size and location of the 7 km domain has been considered large enough

139 to take into consideration all possible synoptic situations relevant for the development

140 of extreme phenomena in the study area as well as the influence of the Mediterranean

141 Sea. The finest nest at 0.025º (circa 2.8 km) covers 150 x 150 grid points, thus a total

142 area of 22500 grid points and includes the study area (72 grid point in x direction and

143 92 in y direction) centred around the Dead Sea.

144 A Tiedtke (1989) mass-flux scheme is used for moist convection in the 7 km, and

145 reduced Tiedke mass-flux scheme for shallow convection. Contrary to the CCLM-7 km

146 simulation, where convection is parameterized, in the CCLM-2.8 km convection is

147 explicitly resolved (Doms and Baldauf, 2015), so only the reduced Tiedke mass-flux

148 scheme is used for shallow convection. The model physics includes a cloud physics

149 parameterization with 5 types of hydrometeors (water vapor, cloud water, precipitation

150 water, cloud ice, precipitation ice), a radiative transfer scheme based on a delta-two-

151 stream solution (Ritter and Geleyn, 1992) and a roughness-length dependent surface

152 flux formulation based on modified Businger relations (Businger et al., 1971).

153 Orography data from GLOBE (Global Land One-km Base Elevation Project) of NOAA

154 (National Oceanic and Atmospheric Administration) and soil data from HWSD

155 (Harmonized Worlds Soil Database) TERRA is used. HWSD is a global harmonization

156 of multiple regional soil data sets with a spatial resolution of 0.008° (FAO, 2009),

157 resulting in 9 different soil types in the model, namely 'ice and glacier', 'rock / lithosols',

158 'sand', 'sandy loam', 'loam', 'loamy clay', 'clay', 'histosols', and 'water'.

159 Multiple model runs have been performed. A 7 km run from 2003 to 2013 with daily

160 output is used as nesting for two 2.8 km runs over the same time span. The Dead Sea

161 is dried out and replaced with soil types from the surrounding area in one of them

162 (SEN), the other one is used as reference (CLIM). For the detailed investigation of

163 convective events on 14.11.2011 and 19.11.2011, sub-seasonal simulations have been

164 performed with the same settings as the decadal simulation, but with additional hourly

165 output.

166 **2.2 Methodology**

167 A decadal simulation covering the 2003 to 2013 time period was carried out with the

168 convection permitting 2.8 km COSMO-CLM model. Lateral boundary conditions and

169 initial conditions are derived from the European Centre for Medium-Range Weather

170 Forecasts (ECMWF) data. The COSMO-CLM 7 km is used as nesting step in between

the forcing data and the 2.8 km run. This reference ~~simulation~~or Dead Sea simulation, will be hereafter referred to as REF^{CLIM} simulation. Parallel to this, an idealized sensitivity experiment (hereafter SEN^{CLIM}, or bare soil simulation) is carried out in which the Dead Sea ~~is dried out~~conditions are ~~and~~ set to bare soil on -405 m level (depth of the Dead Sea in the external data set, GLOBE (Hastings and Dunbar, 1999)). After examination of the results, the first year of simulations is considered spin-up time, thus, our analysis covers the 2004-2013 period.

The precipitation field has been validated using the EOBS dataset (resolution of 0.1° and available for the period 1980-2011; Haylock et al. 2008), and the APHRODITE's (Asian Precipitation - Highly-Resolved Observational Data Integration Towards Evaluation: Yatagai et al. 2008, 2012) daily gridded precipitation, resolution of 0.25° and available for 1980-2007. The APHRODITE data shows generalized lower precipitation values than EOBS, but still higher than our simulation particularly close to the northern Mediterranean shoreline, over coastal-flat terrain, whereas the best agreement is at areas dominated by complex terrain. Despite these biases the comparison of the temporal areal-mean of the model simulations at 7 km and 2.8 km and the APHRODITE dataset demonstrates that in general the model quite well captures the precipitation events. An improvement is seen at the finer resolution.

Regional dry and wet periods are identified and quantified in the simulations by means of the Effective Drought Index (EDI; Byun and Wilhite 1999; Byun and Kim 2010). The EDI is an intensive measure that considers daily water accumulations with a weighting function for time passage normalizing accumulated precipitation. The values are accumulated at different time scales and converted to standard deviations with respect to the average values. Here we use an accumulation period of 365 days. EDI dry and wet periods are categorized as follows: moderate dry periods $-1.5 < EDI < -1$, severe dry periods $-2 < EDI < -1.5$, and extreme dry periods $EDI < -2$. Normal periods are revealed by $-1 < EDI < 1$ values.

Based on daily mean values, precipitation and evapotranspiration distribution and possible tendencies in the 10-year period are assessed. To further asses the most affected areas in our study area, this is divided in four subdomains surrounding the Dead Sea and trying to respect the orographic pattern in the area (Figure 3). Annual cycles are thus separately investigated to take into consideration the relevant differences in orography, soil types, and distance to the coast among others (Figure1), which are known to have a significant impact in the precipitation distribution in the region (e.g. Belachsen 2017; Houze 2012). . Differences in the annual cycle and

206 temporal evolution of precipitation and evapotranspiration between the REF[CLIM] and
207 SEN[CLIM] are discussed. Also, differences in the near-surface and boundary layer
208 conditions and geopotential height patterns are examined. Geographical patterns of
209 mean evapotranspiration and precipitation and differences with respect to the reference
210 or Dead Sea simulation are assessed. Probability distribution functions (PDFs), and the
211 Structure, Amplitude and Location (SAL: Wernli et al. 2008) analysis methodologies are
212 used to illustrate differences in the mean and extreme precipitation between the
213 reference and the sensitivity experiments. The SAL is an object-based rainfall
214 verification method. This index provides a quality measure for the verification of
215 quantitative precipitation forecasts considering three relevant aspects of precipitation
216 pattern: the structure (S), the amplitude (A), and the location (L). The A component
217 measures the relative deviation of the domain-averaged rainfall; positive values
218 indicate an overestimation of total precipitation, negative values an underestimation.
219 The component L measures the distance of the center of mass of precipitation from the
220 modelled one, and the average distance of each object from the center of mass. The
221 component S is constructed in such a way that positive values occur if precipitation
222 objects are too large and/or too flat and negative values if the objects are too small
223 and/or too peaked, quantifying the physical distance between the centres of mass of
224 the two rainfall fields to be compared. Perfect agreement between prediction and
225 reference are characterized by zero values for all components of SAL. Values for the
226 amplitude and structure are in the range (−2, 2), where ±0.66 represents a factor of 2
227 error. The location component ranges from 0 to 2, where larger values indicate a
228 greater separation between centres of mass of the two rainfall fields. This is done by
229 selecting a threshold value of 1/15 of the maximum rainfall accumulation in the domain
230 (following Wernli et al. 2008). The structure and location components are thus
231 independent of the total rainfall in the domain.
232

233 Differences in the temporal evolution of precipitation between the REF[CLIM] and SEN[CLIM]
234 are identified. In Table 1, those events in which an area-mean (study area, Figure 1)
235 difference between both simulations higher than ±0.1 mm/d exists are selected as
236 potential heavy precipitation events and classified attending to their synoptic scale
237 environment and atmospheric stability conditions (Table 1).

238 Although Dayan and Morin (2006) discuss that in general large-scale vertical motions
239 do not provide the sufficient lifting necessary to initiate convection, it was demonstrated
240 by Dayan and Sharon (1980) that a relationship exists between the synoptic-scale
241 weather systems and deep moist convection, being those systems responsible for the

242   moisturizing and destabilization of the atmosphere prior to convective initiation. They

243   pointed out that indices of instability proved the most efficient determinants of the

244   environment characterizing each rainfall type in the region. Thus, two indicators of the

245   atmospheric degree of stability/instability, namely the Convective Available Potential

246   Energy (CAPE; Moncrieff and Miller 1976) and the KO-index (Andersson et al. 1989),

247   are examined in this study. The CAPE is a widely known index indicating the degree of

248   conditional instability. Whereas, the KO-index, which is estimated based on the

249   equivalent potential temperature at 500, 700, 850 and 1000 hPa (following the

250   recommendations by Bolton 1980), describes the potential of deep convection to occur

251   as a consequence of large-scale forcing (Andersson et al. 1989; Khodayar et al. 2013).

252   Generally, regions with KO-index < 2 K and large-scale lifting are identified as

253   favourable for deep convection. Parcel theory (50 hPa ML (Mixed Layer) parcel) and

254   virtual temperature correction (Doswell and Rasmussen 1994) are applied to these

255   calculations.

256   Based on the above criteria, a separation was made between events with widespread

257   rainfall and those more localized. Among the latter, we selected two events to illustrate

258   the local impacts on the boundary layer conducive to deep moist convection.

259   Particularly, differences in the amount, structure and location of precipitation are

260   assessed by examining the spatial patterns and the SAL verification method. The two

261   selected events for detail analysis in this study are those showing the larger SAL

262   deviations. Those two cases occur close in time, but they are not the same event. No

263   differences in the soil and atmospheric conditions have been found in the period

264   between the events when the REF and SEN simulations are compared.   Even though

265   a more detail analysis is provided for the two selected cases, all convective-events

266   listed in Table 1 have been examined to assess the main impacts on the mechanisms

267   leading to convection. High-resolution simulations with the NWP COSMO 2.8 km model

268   are performed with hourly output temporal resolution and covering a 3-day period

269   (including 48-h prior to the day of the event, from 00 UTC) to capture atmospheric pre-

270   conditions conducive to deep moist convection.   For this, a reference simulation,

271   REF^{NWP}, or Dead Sea simulation, and a sensitivity experiment, SEN^{NWP}, or bare soil

272   simulation, are carried out for each event.

273   We have to point out that the external data sets commonly employed describing

274   relevant features of the Dead Sea region, such as the depth, shape and orography of

275   the Dead Sea, as well as Dead Sea water characteristics at the reference or Dead Sea

276   run, do not accurately represent the reality. In the same direction, biases in relation to

277 different variables such as the precipitation field and evaporation over the Dead Sea
278 have to be considered.

279

280 **3. Results and discussion**

281 **3.1 Climatology of the Dead Sea region**

282 *Annual cycle*

283 To assess the climatology of the study region (Figure 1) the annual evaporation and
284 precipitation cycles based on daily means of the respective quantities are investigated
285 (Figure 2). Additionally, we examine the evolution of specific humidity (Qv_{2m}) and
286 temperature at 2 m (T_{2m}) as well as total column integrated water vapour (IWV) and
287 low-boundary layer (< 900 hPa) equivalent potential temperature (Θ_e). Possible
288 changes in the atmospheric stability conditions are evaluated by examination of the
289 CAPE and KO-index. In Figure 2, all grid points over the study region (Figure 1) and
290 the time period 2004-2013 are considered. Differences between the REF^{CLIM} and the
291 SEN^{CLIM} simulations are also discussed.

292 The annual cycle of evaporation shows minimum values in the autumn season (around
293 October, ~ 0.1 mm/d) and maximum evaporation in spring (around March, ~ 0.4 mm/d).
294 The dependency with the precipitation cycle is clear with maximum values of the latter
295 around March and rain occurring between October and May (Figure 2a) in agreement
296 with observations in the area (Dayan and Sharon 1980). The difference between the
297 evaporation in the REF^{CLIM} and the SEN^{CLIM} simulations indicates a mean decrease in
298 the order of 0.02 (February) to ~ 0.1 (August) mm/d in the absence of the Dead Sea
299 water (SEN^{CLIM}). The largest difference is in the dry period (May to October) when
300 water availability is less dependent on precipitation, and evaporation is higher over the
301 Dead Sea in contrast to the minimum values over land (Metzger et al. 2017). In
302 general, there is a decrease of about 0.5 % in mean precipitation in the SEN^{CLIM}
303 simulation. In contrast to the differences in evaporation, precipitation differences
304 between the reference or Dead Sea simulation and the sensitivity or bare soil
305 simulation experiment occur in both directions during the rain period, from October to
306 May. Examining the total number over the whole decadal simulation it is seen that the
307 number of dry or wet days (> 0.1 mm/d) or heavy precipitation events is not largely
308 affected in the sensitivity experiment bare soil simulation. In general, the number of dry
309 days increases (fewer wet days) in the SEN^{CLIM} simulation, whereas the number of high
310 intensity events show almost no variation. For each simulation, the difference between

10

311 precipitation and evaporation is negative mainly in spring and summer contributing to
312 the dryness in the region. Furthermore, the difference between the REF^{CLIM} and
313 SEN^{CLIM} simulations indicates that PREC-EVAP is higher in the SEN^{CLIM} simulation
314 probably in relation to the reduced evaporation over the dry sea area and the general
315 decrease in the precipitation amount in the region.

316 In addition to the reduced evaporation and precipitation (about 0.5 %) in the whole
317 domain in the SEN^{CLIM} simulation a drier and warmer lower-troposphere is identified
318 (Figure 2b) in agreement with the observational assessment by Metzger et al. (2017) of
319 the cooling effect of evaporation on air temperature in the region. The annual cycle of
320 IWV and $\Theta_{e<900hPa}$ in Figure 2c show that the impact of the dry Dead Sea resulting
321 evaporation is less pronounced when a deeper atmospheric layer is considered.
322 Indeed, $\Theta_{e<900hPa}$ evolution evidences that the warming effect due to the decreased
323 evaporation in the SEN^{CLIM} simulation is restricted to the near surface.

324 In Figure 2d, the annual cycle of areal mean CAPE displays larger values in the period
325 from August to November, being this the period more favourable for convection.
326 Negative CAPE differences between the REF^{CLIM} and the SEN^{CLIM} simulations are
327 presumably in relation to the identified distinct lower-atmospheric conditions, being
328 these more favourable and consequently CAPE values higher in the REF^{CLIM}
329 simulation. In the same period, the KO-index indicates a more potentially unstable
330 atmosphere, i.e. prone to deep convection because of large-scale forcing, and larger
331 differences between simulations.

332 In agreement with the well-known precipitation distribution in the region most of the
333 events occur in A1 (north-west) and A2 (north-east). Also, in these subdomains larger
334 differences between the REF^{CLIM} and SEN^{CLIM} simulations are identified pointing out the
335 relevance of the Dead Sea evaporation in the pre-convective environment for rainfall
336 episodes over the study area (Figure3a). Considering only land grid points almost no
337 difference between simulations is found in the evaporation annual cycle of A1 and A2
338 (Figure3b) suggesting the distinct amount of moisture advected towards A1 and A2
339 from the Dead Sea in REF^{CLIM} and SEN^{CLIM} as responsible for the differences in the
340 boundary layer conditions conducive to convection. Also, in these subdomains the
341 dryer and warmer lower boundary layer and the reduced instability in the SEN^{CLIM} are
342 recognized

343 *Inter-annual variability*

11

344   In Figures 4 we discuss the inter-annual variability (based on monthly-daily areal mean
345   values) of evaporation, precipitation as well as drought evolution.

346   The reduced evaporation in the annual cycle of the SEN^{CLIM} simulation for the whole
347   investigation domain, resulting from the drying of the Dead Sea and affected
348   evaporation, remains from year to year (Figure 4a). Larger differences between the
349   simulations occur in the May to November months in agreement with the annual cycle
350   in Figure 2a. This, and the time period of the maximum/minimum is constant over the
351   years. A tendency towards lower evaporation at each simulation and higher differences
352   between both at the end of the period are identified. An inter-annual fluctuation is
353   observed in both REF^{CLIM} and SEN^{CLIM} simulations. The yearly rate of evaporation
354   shows, for example, in REF^{CLIM} maximum values of about 7 mm in 2011 and around 17
355   mm in 2012. This is in agreement with the positive correlation expected between
356   precipitation and evaporation, a trend towards decreased precipitation and a
357   correspondence between drier years such as the 2011-2012 period and lower annual
358   evaporation are seen in Figure 4b. Year to year EDI calculations in Figure 4c help us
359   identify the regional extreme dry and wet periods. The EDI range of variation from
360   about -1 to 2 for the whole period of simulation indicates that the dry condition is the
361   common environment in the area, while the wet periods, EDI up to 6, could be
362   identified as extreme wet periods (relative to the area), in this case in the form of heavy
363   precipitation events. Maximum positive EDI values are in the first months of the year in
364   agreement with the precipitation annual cycle in Figure 2, whereas minimal EDI values
365   occur in summer and autumn indicative of the dry conditions in these periods.
366   Differences in the EDI calculations from both simulations reveal distinct precipitation
367   evolutions and denote timing differences in the occurrence of the precipitation events.
368   When the regional climate evolution is examined in combination with the impact on the
369   number of heavy precipitation events (Table 1) the impact is stronger in the dry period
370   of 2011 (Figure 4a). About six events show relevant differences in this period, contrary
371   to the average 3 episodes per year.

372   *Spatial distribution*

373   The geographical patterns of evaporation and precipitation are presented in Figure 5.
374   Over the Dead Sea, the simulated average annual evaporation for the period under
375   consideration is in the order of 1500-1800 mm/y, in contrast to the values in the deserts
376   east and south, where the evaporation is less than 20 mm/y. Observed annual
377   evaporation of this lake is known to be about 1500 mm and to vary with the salinity at
378   the surface of the lake and freshening by the water inflow (Dayan and Morin 2006;

379 Hamdani et al. 2018). Over land, higher evaporation is seen over the Judean
380 Mountains and the Jordanian Highlands. High correlation with the orography and soil
381 types is seen (Figure 1). Evaporation is probably correlated with rainfall which in turn is
382 correlated with topography. Particularly, in the Jordanian Highlands where maximum
383 evaporation is around 200 mm/y, the complex topography coincides with sandy loam
384 soils, whereas most of the soil in study region is defined as loamy clay or clay (Figure
385 1). The evaporative difference field between simulations in Figure 5a shows a highly
386 inhomogeneous patchiness not evidencing any relationship with orography or soil type,
387 but rather with changes in the precipitation pattern in the SEN^{CLIM} simulation as seen in
388 Figure 5b.

389 In agreement with the temporal series of areal mean precipitation in Figure 3 higher
390 annual precipitation are in the north-west and -east, with respect to the southern
391 regions. Topographic features exert a large impact on precipitation distribution with
392 maxima of about 175 to 300 mm/y over the Judean Mountains and the Jordanian
393 Highlands. To the northern end of the Dead Sea valley, the largest precipitation
394 difference between the REF^{CLIM} and the SEN^{CLIM} simulations is identified, rather than
395 directly over the Dead Sea area noting the importance of advected moisture from the
396 Dead Sea evaporative flux upslope and along the Dead Sea valley as well as the
397 indirect effects of a different spatial distribution of low-tropospheric water vapour in the
398 occurrence of precipitating convection.

399 Regarding the impact on the large-scale conditions, differences in the spatial pattern
400 and strength of the 500 hPa geopotential height field are identified over the Dead Sea
401 (not shown). In the 10-year mean, differences up to 0.002gpdm higher in SEN than in
402 REF are observed. Around the Dead Sea area, the differences are smaller and more
403 irregular. Generally, the differences are higher in the east of the Dead Sea than in the
404 west.

405 *Precipitation probability distribution function*

406 While the probability for lower intensity precipitation is very similar in the REF^{CLIM} and
407 the SEN^{CLIM} simulations differences are recognized in the higher precipitation
408 intensities, from about 150 mm/d (Figure 6a). Particularly, above 180 mm/d extreme
409 precipitation values occur less frequent at the SEN^{CLIM} simulation where a drier,
410 warmer and more stable atmosphere is identified (Figure 2).

411 *SAL*

The use of the SAL method in this study differs from the approach frequently presented in literature since it is here not our purpose to examine differences between the simulated field and observations (adequate observations for this comparison are not available in the area), but to compare changes regarding the structure, amount and location of the precipitation field between our reference or Dead Sea simulation and sensitivity or bare soil simulation experiments. Figure 6b shows that when the mean precipitation over the whole simulation period is considered all three SAL components are close to zero, meaning that very small differences are found. However, when single precipitation events in the REF^{CLIM} simulation are compared with the same period at the SEN^{CLIM} simulation, larger differences regarding structure, amount and location of rainfall events are found. For further examination of this issue two exemplary heavy precipitation events (indicated by boxes in Figure 6b) are analysed in detail. In both cases, a negative A-component is recognized, that is, less precipitation falls in the SEN^{CLIM} simulation. The S-component also evidences the change in the structure of the convective cells. The L-component is low meaning that the convective location does not change significantly in the SEN^{CLIM} simulation, in contrast to the intensity and structure of the cells.

3.2 Sensitivity of atmospheric conditions to the Dead Sea drying: episodic investigation

Among those events exhibiting differences in the precipitation field between both simulations (Table 1 and Figure 6b) two situations occurring in the time period of the 14 to 19 November 2011 are investigated in the following.

In this term, the synoptic situation is characterized by a Cyprus low and its frontal system located over the Dead Sea at about 00 UTC on the 15 November 2011 and at 12 UTC on the 18 November 2011. The low-pressure system and its frontal system induced strong south-westerly to westerly winds with mean wind velocities up to 15 m/s.

In the first situation (hereafter CASE1), in association with the western movement of the cold front a convective system develops over the Jordanian Highlands with precipitation starting at about 21 UTC on the 14 November 2011. This convective system is of high interest because of the large difference in its development between the $REF^{14.11}$ and the $SEN^{14.11}$ simulations.

445   In Figure 7a the 24-h accumulated precipitation, from 14.11 09 UTC to 15.11 08 UTC,
446   in the investigation area is shown for the REF[14.11] and the SEN[14.11] simulations. Two
447   precipitation areas are seen, on the north-western and north-eastern of the Dead Sea.
448   Larger difference between models is on the north-eastern region (24-h accumulated
449   precipitation > 100 mm/d in REF[14.11], while < 50 mm/d in SEN[14.11]), which is the focus of
450   our analysis.

451

452   The REF[14.11] simulation shows that in the 6 hours period prior to the initiation of
453   convection the pre-convective atmosphere and more specifically the lower boundary
454   layer exhibit a moist (IWV ~ 24-30 mm, qvPBLmax ~ 7-10 g/kg) and unstable (CAPE ~
455   1100 J/kg; KO-index ~ -8 K; not shown) air mass on the western side of the
456   investigation area, particularly close to the western Mediterranean coast, and drier
457   (IWV~ 8-16; qvPBLmax ~ 4-6 g/kg) and more stable conditions (CAPE< 200 J/kg; KO-
458   index ~ 0-2 K) on the eastern side of the domain (Figure 7b). A maximum difference of
459   about 5 g/kg from west to east is established in the lower boundary layer.
460   Main differences between both simulations are over the Dead Sea (IWV difference up
461   to 2 mm and qvPBL up to 1.5 g/kg) and north and north-east of it, but almost similar
462   conditions everywhere else. In our target area (subdomain of investigation where the
463   convection episode takes place (red box in Figure 7)), north-east of the Dead Sea, a
464   drier and a more stable atmosphere is identified at the SEN[14.11] simulation.
465   The evolution of the wind circulation systems in the area is similar in both simulations
466   (Figure 7c). The 700 hPa, 850 and 950 hPa winds dominantly blow from the south
467   south-west during the pre-convective environment advecting the moist unstable air
468   mass towards the Dead Sea valley and north-east of it, directly affecting the
469   atmospheric conditions at the target area (for a comparison with a climatology of the
470   wind conditions in the region please see Metzger et al. 2017). In both simulations, the
471   passage of the cold front over the Dead Sea establishes a strong southerly wind from
472   about 10 UTC on the 14 November 2011.
473   Prior to this time, dry air was advected below about 850 hPa towards the target area
474   from the east. The turning of the low-level winds and the resulting moistening of the
475   atmosphere is well and equally captured by both simulations (Figure 8a). Furthermore,
476   at the near-surface, from about 16 UTC, ~ 5 h prior to convection initiation in the target
477   area, a near-surface convergence line forms at the foothills of the northern part of the
478   Jordanian Highlands, which is also well and equally captured by both simulations
479   (Figure 8b). The lifting provided by the convergence line triggers convection in the
480   area. However, the drier and more stable atmosphere in the SEN[14.11]simulation results

481 in less intense convection, weaker updrafts, and reduced precipitation at the eastern
482 slope of the valley.
483

484 In the second case, CASE2, we address an episode of localized convection taking
485 place on the north-western edge of the Dead Sea in the REF simulation, whereas no
486 convection develops in the SEN simulation. The isolated convection in the REF
487 simulation left about 50 mm rain in 3 h starting at about 03 UTC on the 19 November
488 2011 (Figure 9).

489 In contrast to CASE1, the modification of the pre-convective environment relevant for
490 convective initiation is in this case dominated by dynamical changes in the mesoscale
491 circulations. Differences in the evolution and strength of the Mediterranean Sea Breeze
492 (MSB), the Dead Sea breeze and orographic winds influence atmospheric conditions in
493 the target area leading to the assistance to or to the absence of convection. The most
494 significant difference observed between the simulations is in the development of a
495 strong near-surface convergence line in the REF simulation (which is not present in the
496 SEN simulation hindering convection in the area), which forms about 2 h before
497 convective initiation (Figure 10).

498 Even in the first hours of the 18 November 2011 differences in the speed and direction
499 of the near-surface winds over the Dead Sea and on the eastern flank of the Jordanian
500 Highlands could be identified. A fundamental difference between simulations occurs
501 from about 17 UTC when strong westerly winds indicating the arrival of the MSB reach
502 the western shore of the Dead Sea. One hour later, in the REF[19.11] run the MSB
503 strongly penetrates the Dead Sea valley reaching as far as the eastern coast in the
504 centre to south areas. However, in the SEN[19.11] simulation the MSB does not penetrate
505 downward, instead strong northerly winds flow along the valley (Figure 10a). Numerous
506 observational and numerical studies carried out to investigate the dynamics of the MSB
507 (e.g. Naor et al. 2017; Vuellers et al. 2018) showed that the downward penetration of
508 the MSB results from temperature differences between the valley air mass, which is
509 warmer than the maritime air mass. An examination of temperature differences along a
510 near-surface north-south valley transect (positions in Figure 10a) indicates a decrease
511 of about 4 ºC at the near-surface over the dried Dead Sea area in contrast to negligible
512 changes on a parallel transect inland, on the western coast of the Dead Sea. These
513 evidences the notorious impact of the absence of water in the valley temperature, thus,
514 gradients in the region. The colder valley temperatures do not favour the downward
515 penetration of the MSB, which strongly affects the atmospheric conditions in the valley.

16

516 Moreover, a north-easterly land breeze is visible from about 20 UTC on the eastern
517 shore of the Dead Sea in the REF[19.11] simulation, but not in the SEN[19.11] simulation
518 (Figure 10b). This situation reflects an interesting case different from the ones
519 generally presented in former investigations in the area (e.g. Alpert et al. 1997 ; and
520 Alpert et al. 2006b) in which due to the recent weakening of the Dead-Sea breeze,
521 mainly because of the drying and shrinking of the Sea, the Mediterranean breeze
522 penetrates stronger and earlier into the Dead-Sea Valley increasing the evaporation
523 because of the strong, hot and dry wind.

524 Mountain downslope winds develop in both simulations from about 22 UTC. One hour
525 later, strong northerly valley flow in the northern part of the Dead Sea contrasts with the
526 westerly flow in the SEN[19.11] simulation (Figure 10c). As the valley cools down during
527 night time in the SEN simulation, T2m decreases about 1 K from 20 UTC to 03 UTC in
528 contrast with the 0.1 K decrease of the Dead Sea in the REF simulation, the
529 temperature gradient weakens and the northerly valley flow present in the REF
530 simulation is absent in the SEN simulation. During the night, the synoptic conditions
531 gain more influence than the local wind systems governing the conditions in the valley
532 during day time. South-easterly winds prevail in the valley in both simulations. Much
533 stronger wind velocities are reached in the REF simulation, confirming the sensitivity of
534 large-scale dynamics to near-surface climate change-induced impacts.

535 The encounter of the north north-westerly and south south-easterly winds over the
536 Dead Sea area in the REF[19.11] simulation induces the formation of a convergence zone,
537 which intensifies and extends offshore over the next hours and determines the location
538 of convective initiation. Meanwhile, homogeneous south-easterly winds are observed in
539 the SEN simulation (Figure 10d).

540 The differences in the wind circulations contribute to a different distribution of the
541 atmospheric conditions in the target area, particularly, low-tropospheric water vapour
542 as seen in the vertical cross sections in Figure 11. The evolution of the atmospheric
543 conditions in the 3-h period prior to convective initiation evidences the deeper and
544 wetter boundary layer in the REF[19.11] simulation at the north-western foothills of the
545 ridge at the Jordanian Highlands. Differences of IWV up to 2 mm, and of instability
546 (CAPE) close to 200 J/kg are found in this area (not shown). This is the location of the
547 convergence line where convective updrafts, which start close to the ground, are
548 triggered reaching a maximum vertical velocity of about 5 m/s above the convergence
549 zone in the REF[19.11] simulation.

550

4. Conclusions

The drying and shrinking of the Dead Sea has been extensively investigated in the last decades from different points of view. This process has been related to significant local climate changes which affect the Dead Sea valley and neighboring regions. The climate of the Dead Sea is very hot and dry. But occasionally the Dead Sea basin is affected by severe convection generating heavy precipitation, which could lead to devastating flash floods.

In this study, high-resolution COSMO model simulations are used to assess the sensitivity of Dead Sea changes on the occurrence of convective precipitation in the region. A set of high-resolution, ~ 2.8 km, climate simulations covering the period 2003 to 2013, and several numerical weather prediction (NWP) runs on an event time scale (~ 48-36 h) are performed over the Dead Sea area. On a decadal time scale, two simulations are carried out. The first "reference or Dead Sea" run ~~with the Dead Sea area~~, and a second idealized run "sensitivity or bare soil" in which the Dead Sea ~~is dried out~~is ~~and~~ set to bare soil. The NWP simulations focus on two heavy precipitation events exhibiting relevant differences between the reference or Dead Sea and the sensitivity or bare soil decadal runs. A total of four simulations are performed in this case.

As the energy balance partitioning of the Earth's surface changes ~~due to the~~ after setting the Dead Sea area to bare soil conditions~~drying of the Dead Sea~~, relevant impacts could be identified in the region. From a climatological point of view, ~~the drying out of the Dead Sea results in~~ less evaporation, higher air temperatures and less precipitation (about 0.5 %) are observed. Reduced evaporation over the Dead Sea occurs from May to October. ~~The cooling effect of evaporation in the neighboring areas results in an increase of T-2m.~~ Atmospheric conditions, such as air temperature and humidity, are mostly affected in the lower-tropospheric levels, which in turn influence atmospheric stability conditions, hence, precipitating convection. In general, the number of dry/wet days is not largely affected by the ~~drying out~~changed conditions of the Dead Sea, although these differences could be larger for hourly precipitation; rather the structure and intensity of the heavier precipitation events is changed. While a general and homogeneous decrease in evaporation is seen at the SEN^{CLIM} simulation, precipitation deviations occur in both directions, which could suggest and impact on the timing of the events. A relevant year to year variability is observed in evaporation-precipitation which indicates the need of long time series of observations to understand local conditions and to validate model simulations.

586

587 The detailed analysis of two heavy precipitation events allowed us to further assess the
588 possible causes and the processes involved regarding the decrease in precipitation
589 intensity or the total omission of convection with respect to the reference or Dead Sea
590 simulation in the absence of the Dead Sea water. Two main components, strongly
591 affected by the drying outchanged conditions of the Dead Sea area, are found to be
592 highly relevant for the understanding of the environmental processes in the Dead Sea
593 region.

594 (a) First, the lower-atmospheric boundary layer conditions. Changes in the energy
595 balance affect the atmosphere through the heat exchange and moisture supply. The
596 drying of the Dead Sea in the SEN simulations and the resulting decrease in local
597 evaporation, impact the Dead Sea Basin conditions and the neighbouring areas. A
598 reduction in boundary layer humidity and an increase in temperature result in a general
599 decrease of atmospheric instability and weaker updrafts indicating reduced deep-
600 convective activity. Main differences on the atmospheric conditions are directly over the
601 Dead Sea, but these conditions are frequently advected to neighbouring areas by the
602 thermally driven wind systems in the region which play a key role for the redistribution
603 of these conditions and the initiation of convection.

604 (b) Secondly, wind systems in the valley. In the arid region of the Dead Sea Basin with
605 varied topography, thermally and dynamically driven wind systems are key features of
606 the local climate. Three different scales of climatic phenomena coexist: The
607 Mediterranean Sea Breeze (MSB), the Dead Sea breeze and the orographic winds,
608 valley-, and slope-winds, which are known to temper the climate in the Dead Sea valley
609 (Shafir and Alpert, 2011). The drying of the Dead Sea in the SEN simulation disturbs
610 the Dead Sea thermally driven wind circulations. The Dead Sea breezes are missing,
611 weaker wind speeds characterize the region and along valley winds are consequently
612 affected. Furthermore, the dynamics of the Mediterranean breeze penetration into the
613 Jordan Valley are affected.

614

615 Consequently, the impacts on convection initiation and development are twofold:
616 (i) Distinct redistribution of atmospheric conditions, locally or remotely, which yields to
617 different atmospheric conditions that in the absence of the Dead Sea result in a
618 reduced moisture availability in the lower atmospheric levels and increased stability
619 hindering convection or reducing the intensity of the events.

620 (ii) Modification of the divergence/convergence field. The absence of the Dead Sea
621 substantially modifies the wind circulation systems over the Dead Sea valley, which
622 leads to the omission of convergence lines which act as triggering mechanism for
623 convection.

624

625 We can conclude that in general the lack of sufficient low-atmospheric moisture ~~in~~
626 ~~relation to the drying out of the Dead Sea~~, the increase of atmospheric stability in
627 addition to an absence or reduction in the intensity of the convergence zones, works
628 against initiation or intensification of precipitating convection in the area. The relevance
629 of the small-scale variability of moisture and the correct definition and location of
630 convergence lines for an accurate representation of convective initiation illustrates the
631 limitation and the lack of adequate observational networks in the area and the need for
632 high-resolution model simulations of boundary layer processes to predict intense and
633 localised convection in the region.

634 These results contribute to gain a better understanding of the sensitivity of local
635 conditions in the Dead Sea valley and neighbouring areas to ~~lake level decline~~changing
636 conditions at the Dead Sea. Energy balance partitioning and wind circulation systems
637 are determinant for local climatic conditions, e.g. temperature and humidity fields as
638 well as aerosol redistribution, therefore, any change should be well understood and
639 properly represented in model simulations of the region. Our results point out, in
640 agreement with past modelling activities in the region, the need to further improve the
641 representation of precipitation fields in the area, particularly close to the Mediterranean
642 coastline. More accurate Mediterranean SST input fields have been suggested as
643 relevant to reduce the model inaccuracies. Furthermore, a more realistic representation
644 of the lake shape, water salinity and temperature, as well as Dead Sea abundance and
645 depth must be addressed to more accurately describe present and expected future
646 conditions. In the present study, limitations found in this direction in relation to model
647 and external data set descriptions, as well as identified biases regarding for example
648 moisture sources for HP in the region, MSB and Dead Sea evaporation, are expected
649 to impact our results, and have to be improved in future efforts in the region. In a
650 further step, the authors will investigate some of these issues in more detail, and will
651 assess the impact of model grid resolution on the horizontal and vertical flow field in the
652 region across scales, including the impact on large-scale dynamics. We will also put
653 emphasis in trying to better understand the dynamics of the MSB ~~under lake level~~
654 ~~decline~~ using high-resolution modelling, especially the contrasting behaviour pointed
655 out in this study. Fine resolution simulations up to 100 m will be performed for this

656 purpose. Furthermore, we will provide a verification of the complex chain of processes
657 in the area using unique measurements in the framework of the interdisciplinary virtual
658 institute Dead Sea Research VEnue (DESERVE; Kottmeier et al., 2016).

659

672

673 **References**

674 Alpert, P., and Shay-EL, Y.,: The Moisture Source for the Winter Cyclones in the
675   Eastern Mediterranean. Israel Meteorological Research Papers, 5, 20-27, 1994.

676 Alpert, P., and Coauthors: Relations between climate variability in the Mediterranean
677   region and the tropics: ENSO, South Asian and African monsoons, hurricanes
678   and Saharan dust. Developments in Earth and Environmental Sciences, 4, 149-
679   177, https://doi.org/10.1016/S1571-9197(06)80005-4, 2006.

680 Alpert, P., Shafir, H., and Issahary, D.,: Recent Changes in the Climate At the Dead
681   Sea – a Preliminary Study. Climatic Change, 37(3), 513-537,
682   https://doi.org/10.1023/A:1005330908974, 1997.

683 Andersson, T., Andersson, M., Jacobsson, C., Nilsson, S.: Thermodynamic
684   indices for forecasting thunderstorms in southern Sweden. Meteorol. Mag.
685   116, 141-146, 1989.

686 Arkin, Y., and Gilat, A.: Dead Sea sinkholes - an ever-developing hazard.
687   Environmental Geology, 39(7), 711-722,
688   https://doi.org/10.1007/s002540050485, 2000.

689 Ashbel, D., and Brooks, C.: The influence of the dead sea on the climate of its
690   neighbourhood. Quarterly Journal of the Royal Meteorological Society, 65(280),
691   185-194, https://doi.org/10.1002/qj.49706528005, 1939.

692 Ban, N., Schmidli, J., and Schär, C.: Evaluation of the convection-resolving
693   regional climate modeling approach in decade-long simulations, J. Geophys.
694   Res. Atmos., 119, 7889– 7907, https://doi.org/10.1002/2014JD021478, 2014.

695 Belachsen, I., Marra, F., Peleg, N., and Morin, E.: Convective rainfall in dry climate:
696   relations with synoptic systems and flash-flood generation in the Dead Sea
697   region. Hydrology and Earth System Sciences Discussions, 21, 5165-5180,
698   https://doi.org/10.5194/hess-21-5165-2017, 2017.

699 Böhm, U., and Coauthors: The Climate Version of LM: Brief Description and Long-
700   Term Applications. COSMO Newsletter, 6, 225-235, 2006.

701 Businger, J., Wyngaard, J., Izumi, Y., and Bradley, E.: Flux-Profile Relationships in the
702   Atmospheric Surface Layer. Journal of the Atmospheric Sciences, 28(2), 181-
703   189, https://doi.org/10.1175/1520-0469(1971)028<0181:FPRITA>2.0.CO;2,
704   1971.

705 Byun, H., and Kim, D.: Comparing the Effective Drought Index and the Standardized
706   Precipitation Index. Options Méditerranéennes. Séries A. Mediterranean
707   Seminars, 95, 85-89, 2010.

708 Byun, H., and Wilhite, D.: Objective quantification of drought severity and duration. J.
709   Climate, 12(9), 2747-2756, https://doi.org/10.1175/1520-
710   0442(1999)012<2747:OQODSA>2.0.CO;2, 1999.

711 Cohen, S., and Stanhill, G.: Contemporary Climate Change in the Jordan Valley. J.
712   Appl. Meteor., 35(7), 1051-1058, https://doi.org/10.1175/1520-
713   0450(1996)035<1051:CCCITJ>2.0.CO;2, 1996.

714 Corsmeier, U., Behrendt, R., Drobinski, P., Kottmeier, C.: The mistral and its
715   effect on air pollution transport and vertical mixing, Atmos. Res., 74, 275–302,
716   https://doi.org/https://doi.org/10.1016/j.atmosres.2004.04.010, 2005.

Código de campo cambiado

717 Dayan, U., and Morin, E.: Flash flood – producing rainstorms over the Dead Sea: A
718 review. Geological Society of America, 401(4), 53-62,
719 https://doi.org/10.1130/2006.2401(04) , 2006.

720 Dayan, U., and Sharon, D.: Meteorological parameters for discriminating between
721 widespread and spotty storms in the Negev. Israel Journal of Earth Sciences,
722 29(4), 253-256, 1980.

723 Dayan, U., Ziv, B., Margalit, A., Morin, E., and Sharon, D.: A severe autumn storm over
724 the middle-east: synoptic and mesoscale convection analysis. Theoretical and
725 Applied Climatology, 69(1-2), 103-122, https://doi.org/10.1007/s007040170038,
726 2001.

727 Doms, G., and Baldauf, M.: A Description of the Nonhydrostatic Regional COSMO-
728 Model. Part I: Dynamics and Numerics. Deutscher Wetterdienst, 2015.

729 Doswell, C., and Rasmussen, E.: The Effect of Neglecting the Virtual Temperature
730 Correction on CAPE Calculations. Weather and Forecasting, 9(4), 625-629,
731 https://doi.org/10.1175/1520-0434(1994)009<0625:TEONTV>2.0.CO;2, 1994.

732 FAO/IIASA/ISRIC/ISSCAS/JRC.: Harmonized World Soil Database (version 1.2). FAO,
733 Rome, Italy and IIASA, Laxenburg, Austria, (accessed 01.02.2017) , 2009.

734 Fosser, G., Khodayar, S., and Berg, P., 2014: Benefit of convection permitting climate
735 model simulations in the representation of convective precipitation, Clim. Dyn.,
736 44(1– 2), 45– 60.

737 Gavrieli, I., Bein, A., and Oren, A., 2005: The expected impact of the "Peace Conduit"
738 project (the Red Sea - Dead Sea pipeline) on the Dead Sea. Mitigation and
739 Adaptation Strategies for Global Change, 10(4), 759-777,
740 https://doi.org/10.1007/s11027-005-5144-z.

741 European Commission, Joint Research Centre, 2003: Global Land Cover 2000
742 database, (accessed 01.02.2017).

743 GLOBE National Geophysical Data Center, 1999: Global Land One-kilometer Base
744 Elevation (GLOBE) v.1. Hastings, D. and P.K. Dunbar. National Geophysical
745 Data Center, NOAA, (accessed 01.02.2017).

746 Greenbaum, N., Ben-Zvi, A., Haviv, I., and Enzel, Y., 2006: The hydrology and
747 paleohydrology of the Dead Sea tributaries. Geological Society of America,
748 401(4), 63-93, https://doi.org/10.1130/2006.2401(05).

749 Haylock, M.R., Hofstra, N., Klein Tank, A.M.G., Klok, E.J., Jones, P.D. and New, M.
750 2008, A European daily high-resolution gridded dataset of surface temperature and
751 precipitation. Journal of Geophysical Research: Atmospheres, 113, D20119.
752 https://doi.org/10.1029/2008JD10201.

753

754 Hochman, A., Mercogliano, P., Alpert, P., Saaroni, H. and Bucchignani, E., 2018. High-
755 resolution projection of climate change and extremity over Israel using COSMO-CLM.
756 International Journal of Climatology, 38(14), pp.5095-5106.

757

758 Houze, R., 2012: Orographic effects on precipitating clouds. Reviews of Geophysics,
759   50(1), https://doi.org/10.1029/2011RG000365.

760 Kalthoff, N., Horlacher, V., Corsmeier, U., Volz-Thomas, A., Kolahgar, B., Geiß, H.,
761   Möllmann-Coers, M., and Knaps, A. 2000: Influence of valley winds on transport
762   and dispersion of airborne pollutants in the Freiburg-Schauinsland area, J.
763   Geophys. Res. Atmos, 105, 1585–1597, https://doi.org/10.1029/1999jd900999.

764
765 Khodayar, S., Kalthoff, N., and Schaedler, G., 2013: The impact of soil moisture
766 variability on seasonal convective precipitation simulations. Part I: validation,
767 feedbacks, and realistic initialisation. Meteorologische Zeitschrift, 22(4), 489-505,
768 https://doi.org/10.1127/0941-2948/2013/0403.

769 Kunin, P., Alpert, P. and Rostkier-Edelstein, D., 2019. Investigation of sea-
770 breeze/foehn in the Dead Sea valley employing high resolution WRF and observations.
771 Atmospheric Research.

772

773 Lensky, N. and Dente, E., 2015. The hydrological proecesses driving the accelerated
774 Dead Sea level decline in the past decades. Geological Survey of Israel Report.

775

776 Llasat, M., and Coauthors, 2010: High-impact floods and flash floods in Mediterranean
777   countries: the FLASH preliminary database. Advances in Geosciences, 23, 47-
778   55, https://doi.org/10.5194/adgeo-23-47-2010.

779 Metzger, J., Nied, M., Corsmeier, U., Kleffmann, J., and Kottmeier, C., 2017: Dead Sea
780   evaporation by eddy covariance measurements versus aerodynamic, energy
781   budget, Priestley-Taylor, and Penman estimates. Hydrology and Earth System
782   Sciences Discussions, 22(2), 1135-1155, https://doi.org/10.5194/hess-2017-
783   187.

24

784 Miglietta MM, Conte D, Mannarini G, Lacorata G, Rotunno R. 2011. Numerical analysis
785 of a Mediterranean 'hurricane' over south-eastern Italy: sensitivity experiments to sea
786 surface temperature. *Atmos. Res.* **101**: 412–426.
787

788 Moncrieff, M., and Miller, M., 1976: The dynamics and simulation of tropical
789 cumulonimbus and squall lines. Quarterly Journal of the Royal Meteorological
790 Society, 102(432), 373-394, https://doi.org/10.1002/qj.49710243208, 2014.

791 Naor, R., Potchter, O., Shafir, H., and Alpert, P.: An observational study of the
792 summer Mediterranean Sea breeze front penetration into the complex
793 topography of the Jordan Rift Valley, Theor. Appl. Climatol., 127, 275–284,
794 https://doi.org/10.1007/s00704-015-1635-3, 2017.

795 Prein, A., Gobiet, A., Suklitsch, M., Truhetz, H., Awan, N., Keuler, K., and Georgievski,
796 G. : Added value of convection permitting seasonal simulations, Clim.
797 Dyn., 41(9– 10), 2655– 2677, 2013.

798 Ritter, B., and J.-F. Geleyn, 1992. A comprehensive radiation scheme for numerical
799 weather prediction models with potential applications in climate simulations. Mon. Wea.
800 Rev., 120, 303–325.

801 Rostkier-Edelstein, D., Liu, Y., Wu, W., Kunin, P., Givati, A. and Ge, M., 2014. Towards
802 a high-resolution climatography of seasonal precipitation over Israel. International
803 Journal of Climatology, 34(6), pp.1964-1979.
804

805 Schaedler, G., and Sasse, R.: Analysis of the connection between precipitation and
806 synoptic scale processes in the Eastern Mediterranean using self-organizing maps.
807 Meteorologische Zeitschrift, 15(3), 273-278, https://doi.org/10.1127/0941-
808 2948/2006/0105, 2006.

809 Shafir, H., and Alpert, P.: Regional and local climatic effects on the Dead-Sea
810 evaporation. Climatic Change, 105(3-4), 455-468,
811 https://doi.org/10.1007/s10584-010-9892-8, 2011.

812 Sharon, D., and Kutiel, H.: The distribution of rainfall intensity in Israel, its regional and
813 seasonal variations and its climatological evaluation. International Journal of
814 Climatology, 6(3), 277-291, https://doi.org/10.1002/joc.3370060304, 1986.

815 Smiatek, G., Kunstmann, H., and Heckl, A.: High-resolution climate change simulations
816   for the Jordan River area. Journal of Geophysical Research, 116(D16),
817   https://doi.org/10.1029/2010JD015313, 2011.

818 Stanhill, G.: Changes in the rate of evaporation from the dead sea. International
819   Journal   of   Climatology,   14(4),   465-471,
820   https://doi.org/10.1002/joc.3370140409,1994.

821 Vicente-Serrano, S., Beguería, S., López-Moreno, J.: A Multiscalar Drought Index
822   Sensitive   to   Global   Warming: The   Standardized   Precipitation
823   Evapotranspiration   Index.   J.   Climate,   23(7),   1696-1718,
824   https://doi.org/10.1175/2009JCLI2909.1, 2010.

825 Vüllers, J., Mayr, G. J., Corsmeier, U., and Kottmeier, C.: Characteristics and
826   evolution of diurnal foehn events in the Dead Sea valley. Atmos. Chem. Phys.,
827   18, 18169-18186, https://doi.org/10.5194/acp-18-18169-2018, 20, 2018.

828

829 Wernli H, Paulat M, Hagen M, Frei C. SAL – a novel quality measure for the
830   verification of quantitative precipitation forecasts. Mon. Weather Rev. 136: 4470–
831   4487, 2008.

832

833 Yatagai, A., Alpert, P. and Xie, P. (2008) Development of a daily gridded precipitation
834 data set for the Middle East. Advances in Geosciences, 12, 1–6.

835

836 Yatagai, A., Kamiguchi, K., Arakawa, O., Hamada, A., Yasutomi, N. and Kitoh, A.,
837 2012: APHRODITE: constructing a long-term daily gridded precipitation dataset for
838 Asia based on a dense network of rain gauges. Bulletin of the American Meteorological
839 Society, 93, 1401–1415.

840

841

842

843

844

845

846

847

848

849

850

851

852

853

854

855

856

857

858

859

860 **Tables**

	PREC diffmn	REF PMX	SEN PMX	PREC relative diff [%]	Synoptic Situation	REF CAPEmx	SEN CAPEmx	REF KOmn	SEN KOmn	Localised/ Widespread (Subarea affected)
08.12.2004	0,10	30,09	31,31	2,76	ARST	1	1	4,85	4,85	W (A1, A2)
13.01.2006	-0,11	45,64	54,64	-4,26	Cyprus Low	239	225	6,57	6,54	L/W (A1, A3)
16.04.2006	0,11	57,41	56,09	4,89	Syrian Low	43	47	1,97	1,94	L (A1, A4)
10.04.2007	0,29	42,61	70,20	30,78	Cyprus Low	686	679	-4,77	-4,70	L (A2, A4)
13.04.2007	0,12	134,36	127,79	1,62	Cyprus Low	573	576	-1,95	-1,92	L (A1, A2, A3, A4)
12.05.2007	-0,16	41,82	47,90	-8,24	Syrian Low	436	81	-5,30	-5,29	L (A1, A2)
27.01.2008	-0,14	23,11	17,24	-17,25	Syrian Low	7	7	5,12	5,12	W (A1, A3)
25.10.2008	-0,23	139,01	125,73	-16,52	ARST	1274	1361	-5,50	-4,08	L (A3)
13.11.2008	0,30	40,83	45,55	25,68	ARST	25	7	1,37	1,38	L (A2, A4)
14.05.2009	-0,39	59,28	68,84	-8,49	Syrian Low	433	429	-3,90	-3,91	L (A1, A2, A3, A4)
15.05.2009	0,20	49,23	42,28	13,50	Syrian Low	208	203	-2,30	-2,36	L (A1, A2, A3)
31.10.2009	-0,19	166,21	111,79	-7,65	Cyprus Low	435	445	-5,03	-4,46	L (A1, A2)
15.01.2011	0,11	73,02	72,03	3,74	Syrian Low	49	37	7,82	7,83	L/W (A1, A4)
28.05.2011	-0,24	44,51	32,73	-14,33	Cyprus Low	158	170	-10,27	-10,26	W (A2)
14.11.2011	-0,11	42,65	9,34	-65,90	Cyprus Low	2	0	-7,14	-7,12	L (A1, A2)
17.11.2011	0,11	90,07	93,04	4,76	Cyprus Low	386	304	-9,14	-9,16	L (A1)
18.11.2011	-0,11	28,68	34,69	-8,67	Cyprus Low	356	378	-8,61	-8,65	L (A1)
19.11.2011	0,03	58,11	12,36	4,09	Cyprus Low	133	81	-7,60	-7,46	L (A2, A4)

22.10.2012	0,20	29,88	41,64	51,21	ARST	2068	2097	-5,83	-5,59	L (A1, A2)
09.11.2012	-0,11	27,20	22,56	-18,29	Cyprus Low	218	215	3,97	3,98	W (A1)
23.11.2012	-0,21	155,77	117,81	-10,17	ARST	189	286	-2,18	-1,95	L (A1, A2, A3)
25.11.2012	-0,11	41,48	54,33	-7,87	ARST	354	332	4,19	4,37	L (A3, A4)

861

862

863 **Table 1:** Classification of heavy precipitation cases in the decadal simulation covering
864 the period 2004 to 2013. The areal-mean (study area, Figure 1) difference ($PREC_{diffmn}$)
865 and maximum grid precipitation in the reference (REF_{PMX}) and sensitivity (SEN_{PMX})
866 realizations, the precipitation relative difference in %, the synoptic situation, and the
867 stability conditions illustrated by maximum grid point CAPE (CAPEmx) and minimum
868 grid point KO-index (KOmn) are summarized. Additionally, the nature of the
869 precipitation, localized (L) or widespread (W) and the main subarea affected (following
870 division in Figure 1; A1, A2, A3, A4) are listed.

871

872

873

874

875

876

877

878

879

880 **Figures**

881 (a)

28

882

883   (b)

884

885
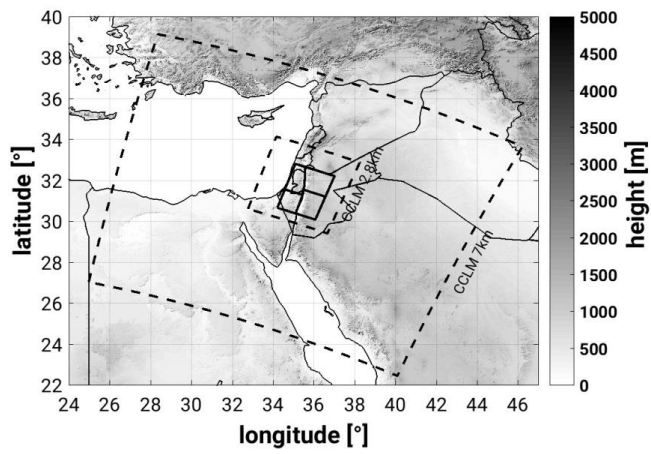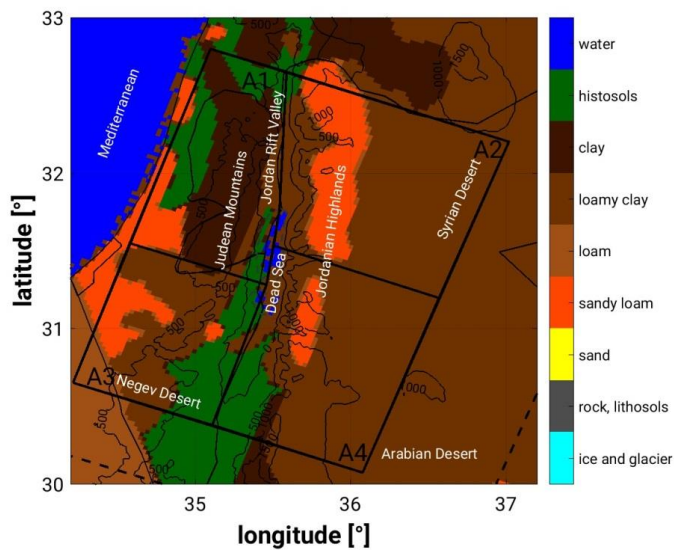
Figure 1: (a) Topography (m above msl), simulation domains (dashed lines, CCLM7km and CCLM2.8km) and study area (bold line). (b) Model soil types (colour scale), topography (black isolines) and study area (black bold line) including the 4 subdomains to be examined, A1-4 (Area 1-4).

890   (a)

891

29

892

893

894

895

896

897

898

899

900

901

902

903   (b)
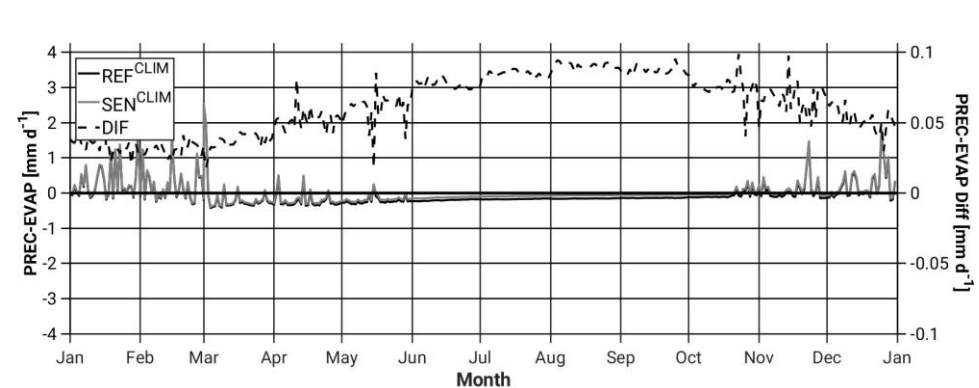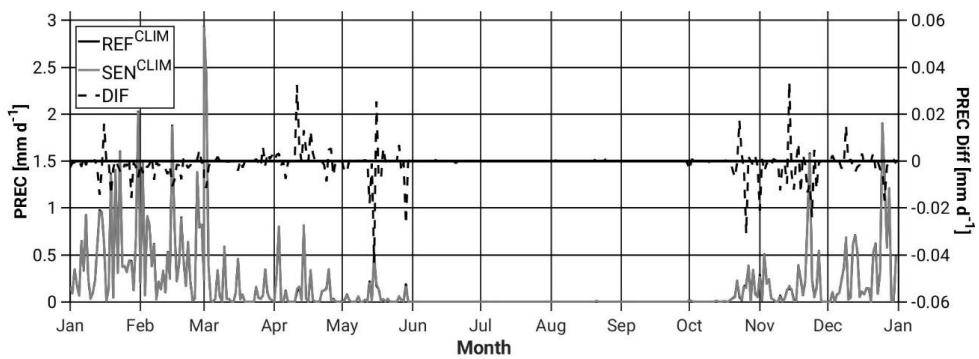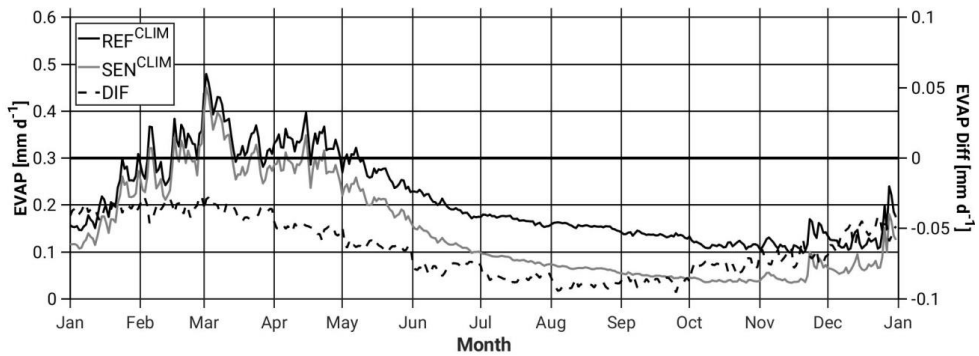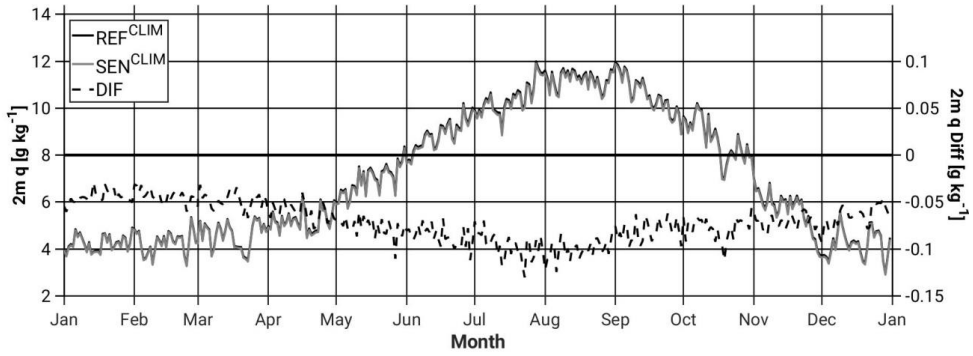
904
905
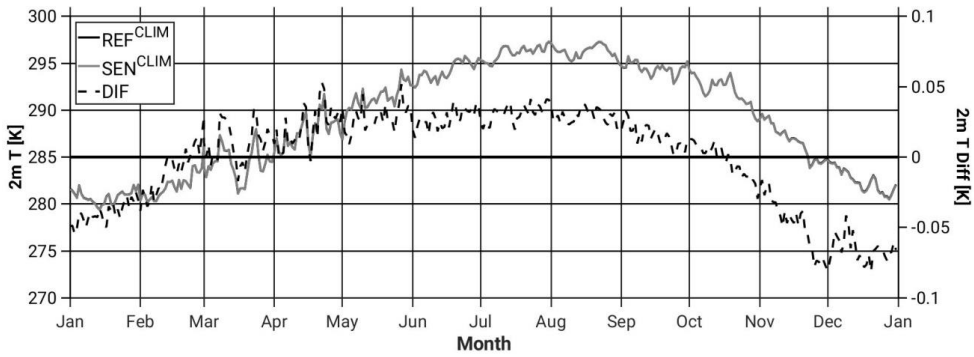
906
907
908
909
910
911
912
913
914
915
916
917
918
919   (c)

920
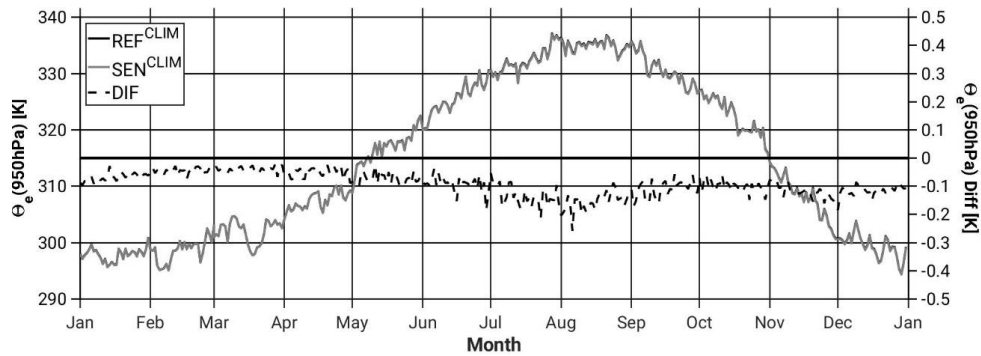
921
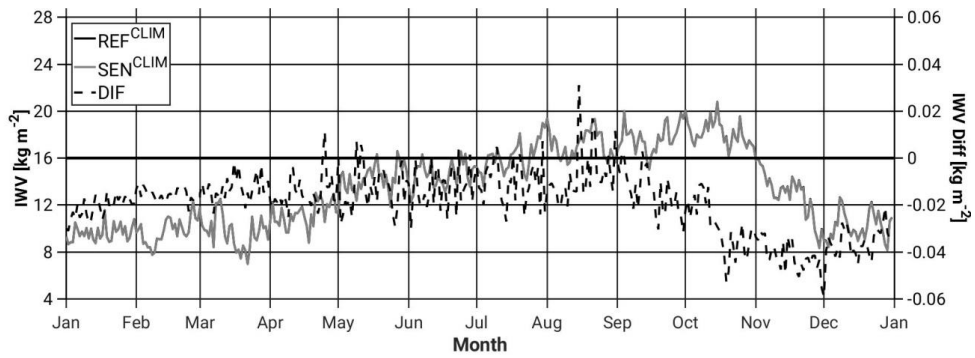
922

923

924

925

926

927

928

929

930

931

932

933

934

935

936

937   (d)

938
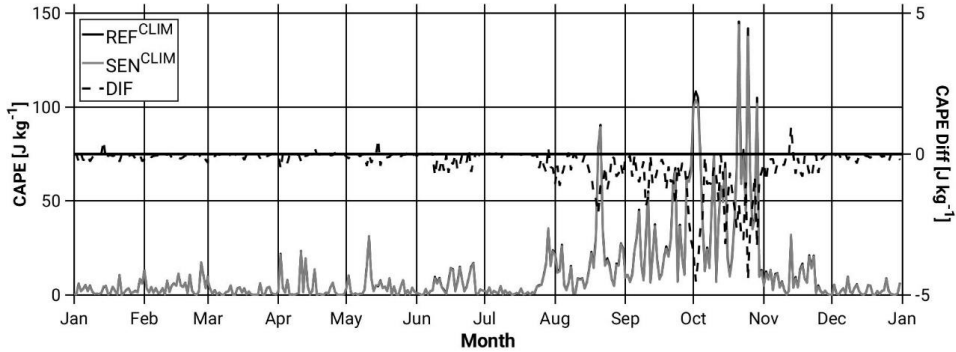
939
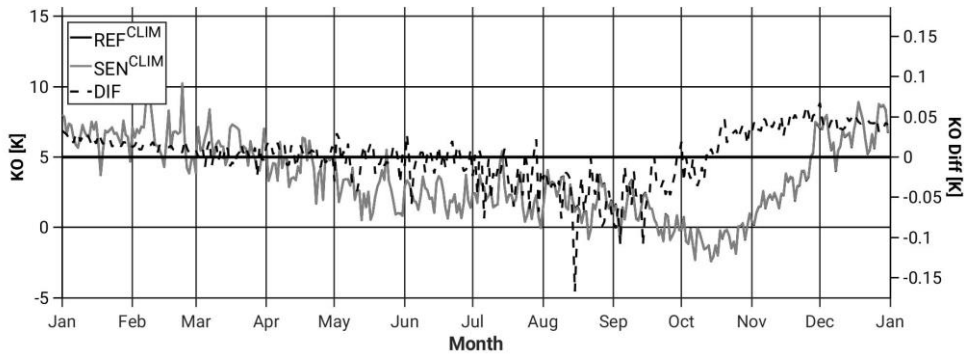
940

941

942

943   Figure 2: Annual cycle of the area-averaged-daily accumulated averaged (and
944   differences (black dashed line; SEN-REF)) of (a) evaporation, precipitation, and
945   precipitation minus evaporation (b) specific humidity and temperature at 2-m, and (c)
946   Θ_e below 950 hPa and IWV, and (d) CAPE and KO-index, from the REF^{CLIM} (full black
947   line) and the SEN^{CLIM} (full grey line) simulations. All grid points in the study area (Figure
948   1) and the period 2004 to 2013 are considered.

949

950

951

952

953

954

955   (a)

956   Area1 (NW)   Area2 (NE)
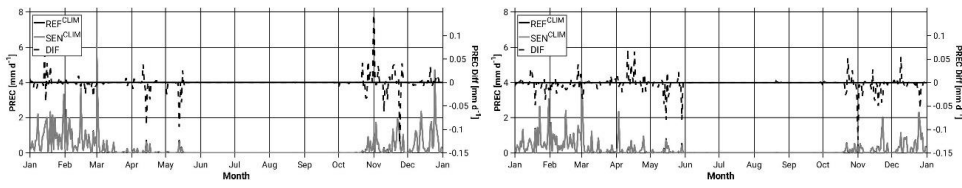
957

958   Area3 (SW)   Area4 (SE)
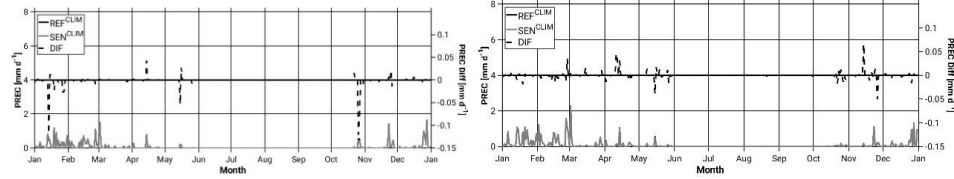
959

960   (b)

961   Area1 (NW)   Area2 (NE)
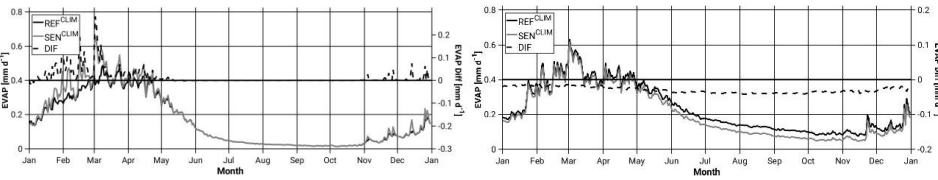
962
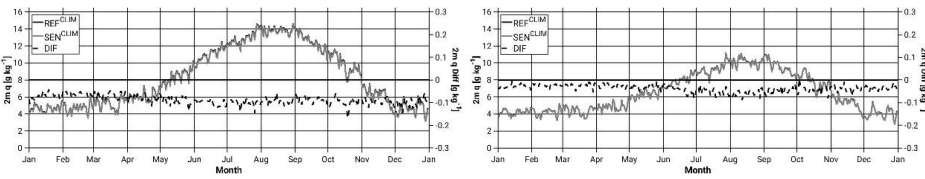
963
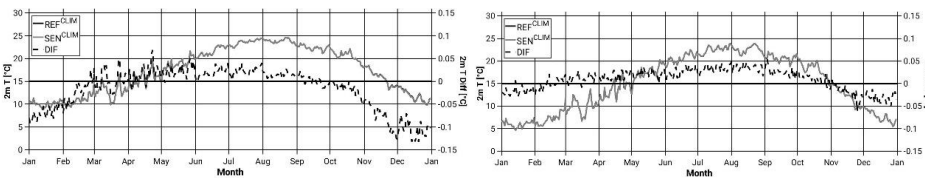
964
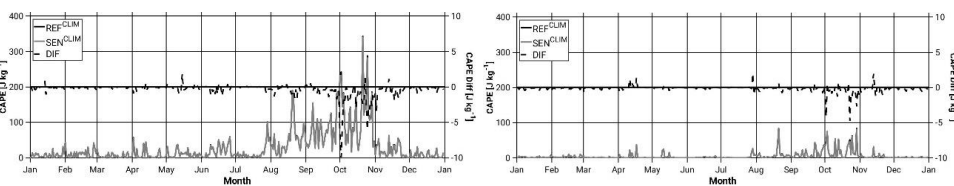
965

966

967

968   Figure 3: Annual cycle of the areal-daily averaged (and differences (black dashed line;
969   SEN-REF)) of (a) precipitation for areas A1, A2, A3, A4 (see Figure 1b), and (b)
970   evaporation, specific humidity and temperature at 2-m, and CAPE for areas A1 and A2,

34

971 from the REF^{CLIM} (full black line) and the SEN^{CLIM} (full grey line) simulations. Only land
972 points in the study area (Figure 1) for evaporation, and all grid points for the rest of
973 variables and the period 2004 to 2013 are considered.

974

975

976

977

978

979

980

981

982

983

984

985

986

987

988

989

990

991

992

993

994

995

996

997

998

999   (a)
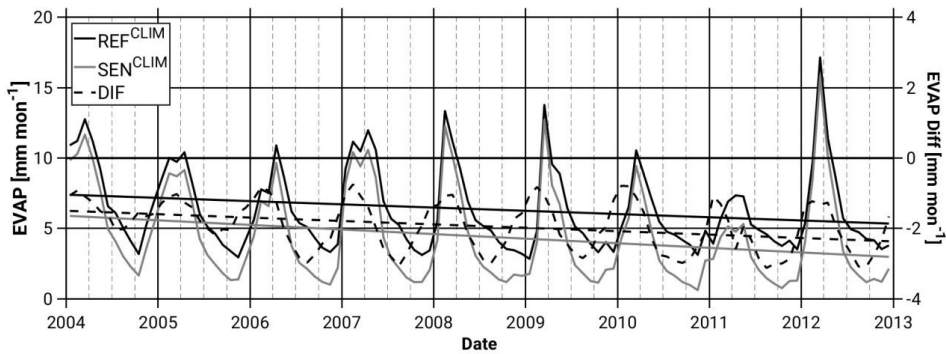
1000

1001   (b)
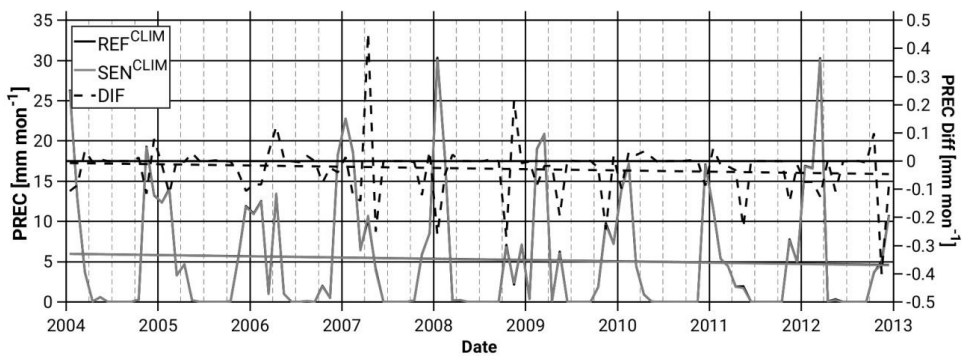
1002

1003   (c)
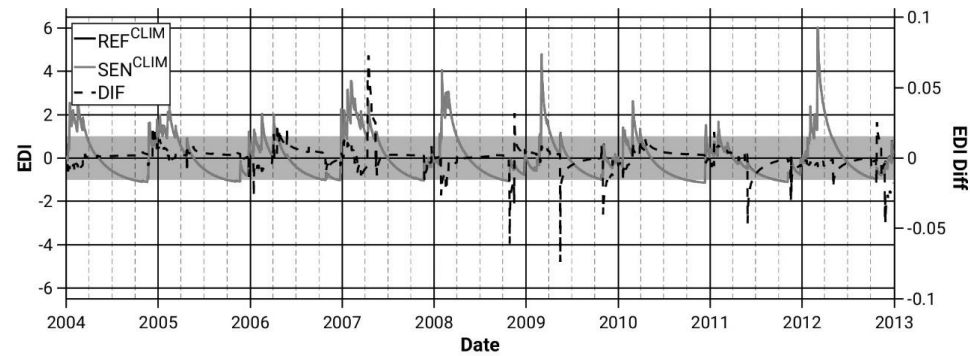
1004

1005   Figure 4: Temporal evolution of the area-averaged monthly-daily accumulated areal
1006   mean values of (a) Evaporation, (b) Precipitation, (c) Effective Drought Index (EDI),
1007   from the REF^{CLIM} (full black line) and the SEN^{CLIM} (full grey line) simulations and
1008   differences depicted with black dashed lines. The light grey band in (c) indicates the
1009   common soil state (-1<EDI<+1). All grid points in the study area (Figure 1) and the
1010   period 2004 to 2013 are considered.

1011

1012

1013   (a)
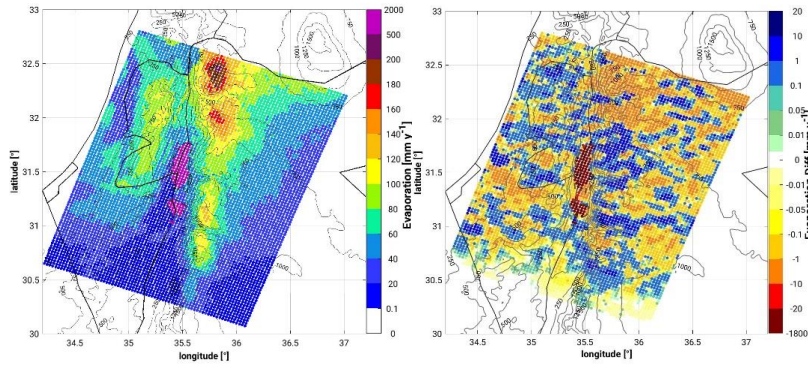
1014

1015

1016

1017   (b)
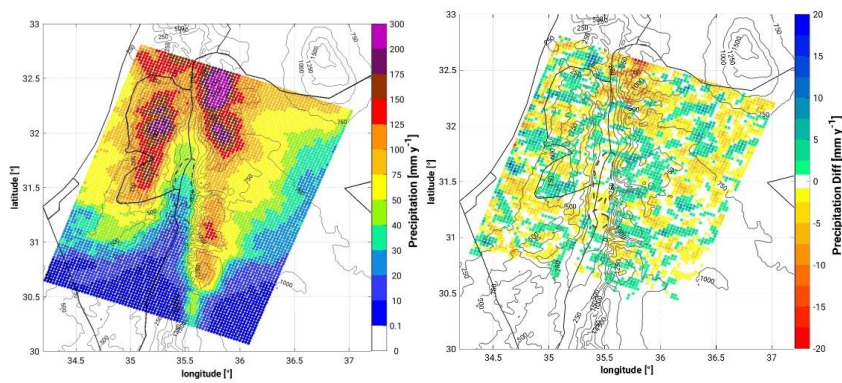
1018

1019

1020

1021   Figure 5: Spatial distribution of (a) evaporation in the REF[CLIM] simulation (left) and the
1022   difference between the SEN[CLIM] and the REF[CLIM] simulations (right), and (b)
1023   precipitation in the REF[CLIM] simulation (left) and the difference between the SEN[CLIM]
1024   and the REF[CLIM] simulations (right). The period 2004 to 2013 is considered.

1025

1026

1027

1028

1029   (a)   (b)
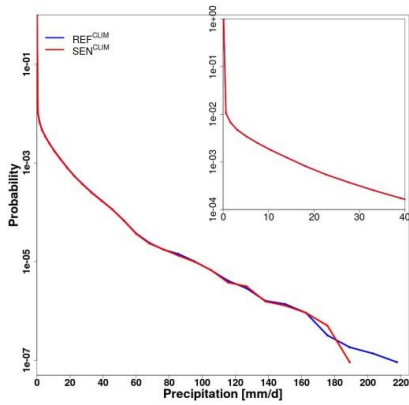
1030

1031

1032
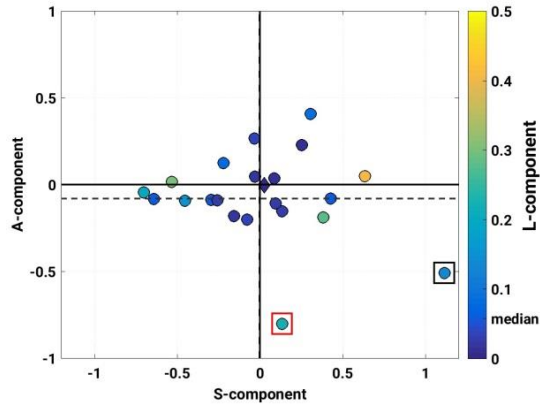
1033   Figure 6: (a) Probability density function of daily precipitation intensities. All grid points
1034   in the investigation domain (Figure 1) and the period 2004 to 2013 are considered. (b)
1035   SAL diagram between REF[CLIM] and SEN[CLIM] simulations. Every circle corresponds to a
1036   simulated heavy precipitation event (listed in Table 1). The diamond (close to the zero-
1037   zero) illustrates the mean of all events. A-component (amplitude), S-component
1038   (structure), L-component (location). The inner colour indicates the L-component. Boxes
1039   point out the two events examined in this study, CASE1 and CASE2 (see section 3.2).

1040

1041

1042

1043

1044

1045

1046

1047

1048

1049

1050

1051

1052

1053   (a)
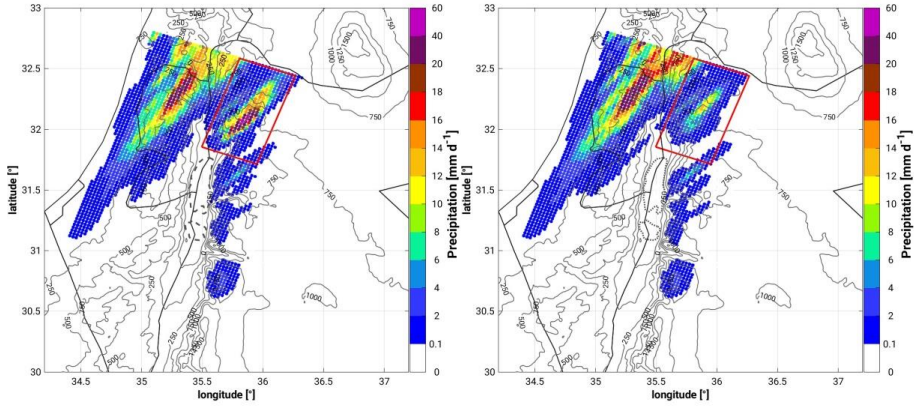
1054

1055   (b)
1056
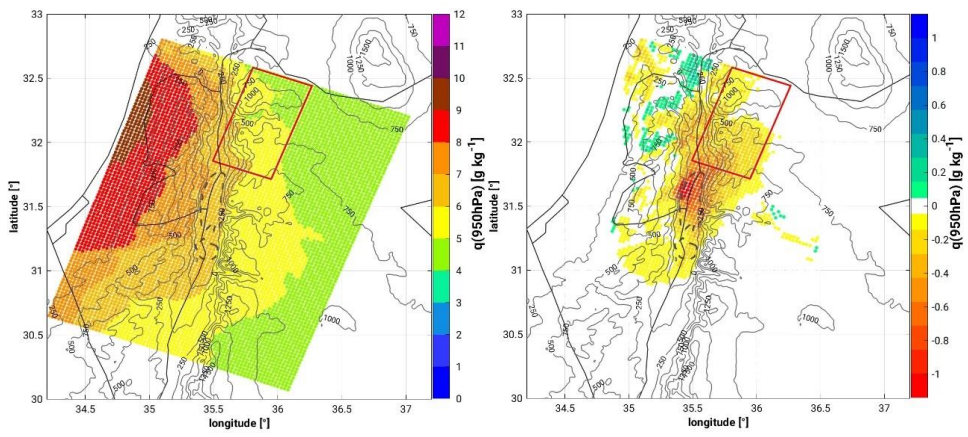
1057
1058

1059

1060

1061

1062

1063

1064

1065

1066   (c)
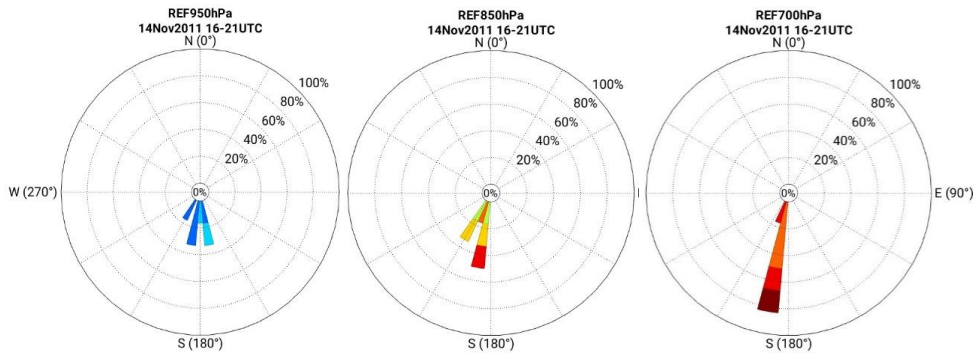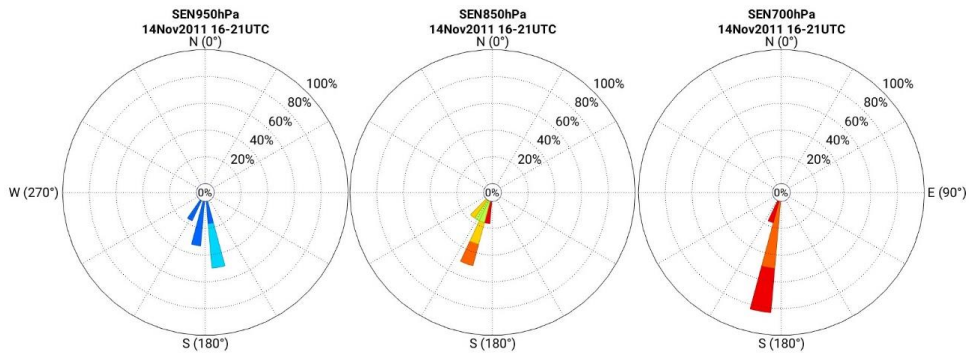
Figure 7: Spatial distribution of (a) 24-h accumulated precipitation from 14.11 09 UTC to 15.11 08 UTC from the REF[14.11] simulation (left) and the SEN[14.11] simulation (right) and (b) specific humidity below 950 hPa, from the REF[14.11] simulation (left) and the

1078   difference between the REF[14.11] and SEN[14.11] simulations, as a mean for the 6-h period
1079   prior to convection initiation in the target area (14 November 16 UTC to 21 UTC), and
1080   (c) wind conditions at 700 hPa, 850 hPa, and 950 hPa (no relevant differences with
1081   respect to the 10-m field) for the same time period. Wind roses are centred at about
1082   35.82°E-32.07°N in our target area.

1083

1084

1085

1086

1087

1088

1089

1090

1091

1092

1093

1094

1095

1096

1097

1098

1099

1100

1101

1102

1103

1104

1105

1106

1107   (a)
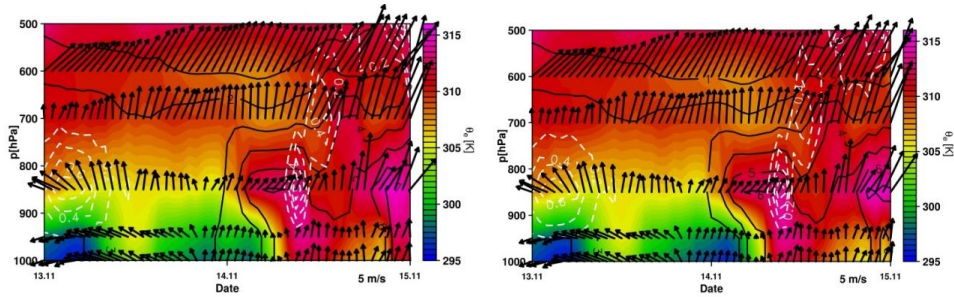
1108

1109   (b)

1110
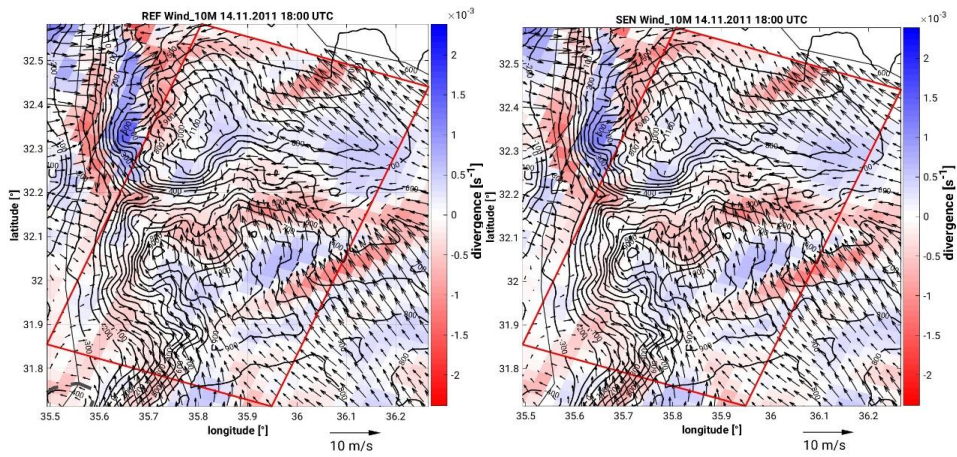
1111

1112

1113   Figure 8: (a) Vertical-temporal cross-section of equivalent potential temperature (colour
1114   scale; K), specific humidity (black isolines; g/kg), horizontal wind vectors (north-pointing
1115   upwards, m/s) and vertical velocity (white dashed contours with 0.1 m/s increments) of
1116   the REF[14.11] (left) and SEN[14.11] (right) simulations, over a representative grid point in the
1117   sub-study region, 32.05°N 35.79°E. (b) Spatial distribution of 10-m horizontal wind
1118   (wind vectors; m/s) and corresponding divergence/convergence field (colour scale; s[-1])
1119   at 18 UTC on the 14 November 2011 from the REF[14.11] (left) and SEN[14.11] (right)
1120   simulations.

1121

1122
1123
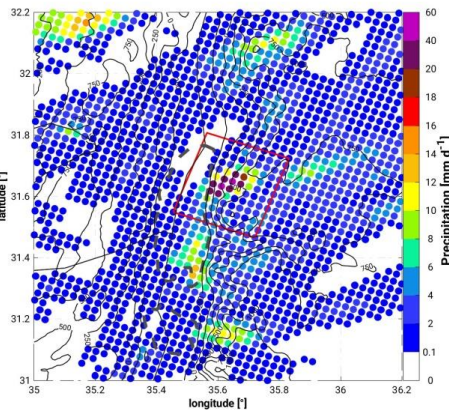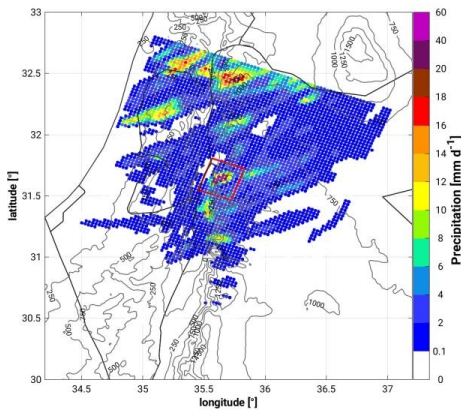
1124
1125
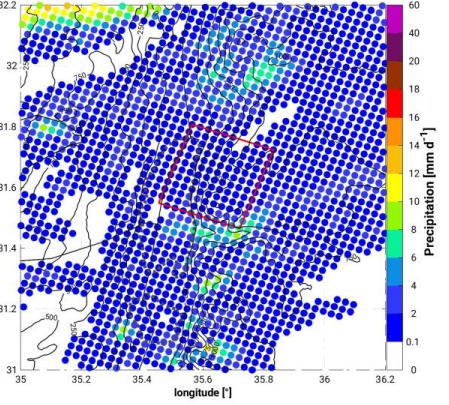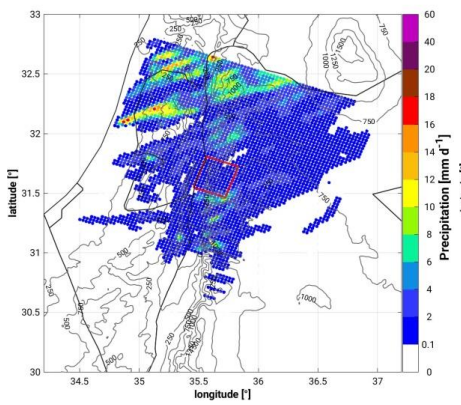
1126
1127
1128
1129

Figure 9: 24-h mean spatial distribution of precipitation from the REF[19.11] simulation (top-left; zoom top-right) and the SEN[19.11] simulation (bottom-left; zoom bottom-right) for the period 18 November 2011 11 UTC to 19 November 2011 10 UTC.

1133

1134

1135
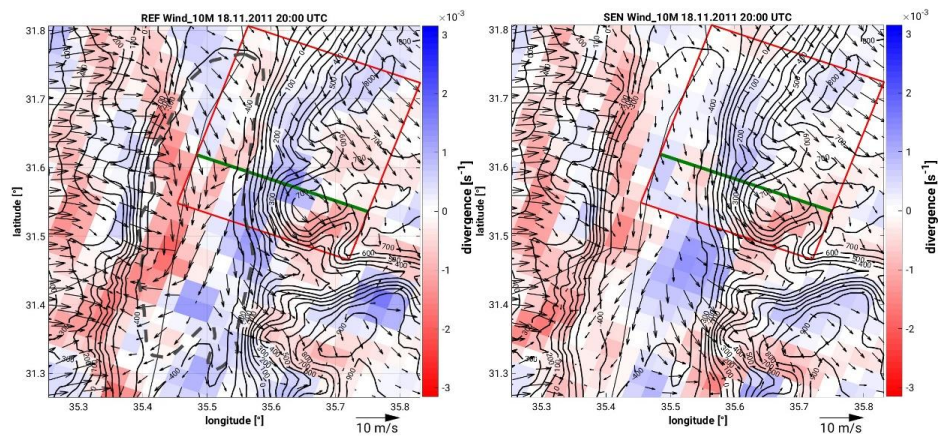
1136

1137

1138

1139

1140

1141   (a)
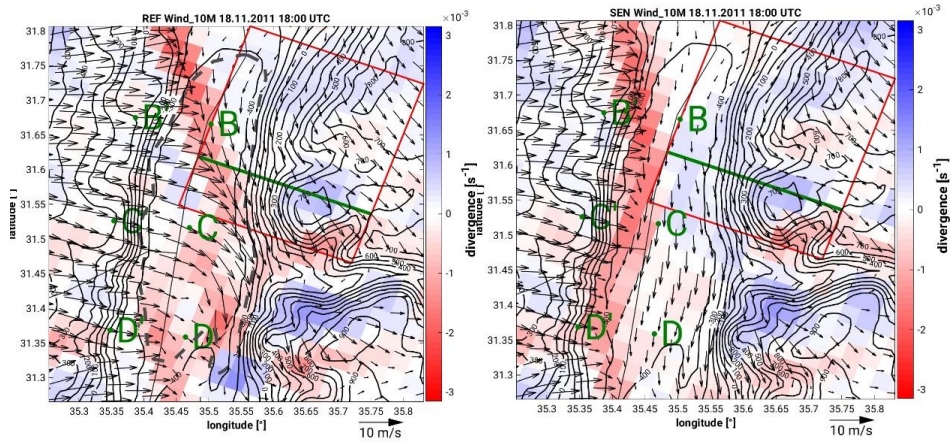
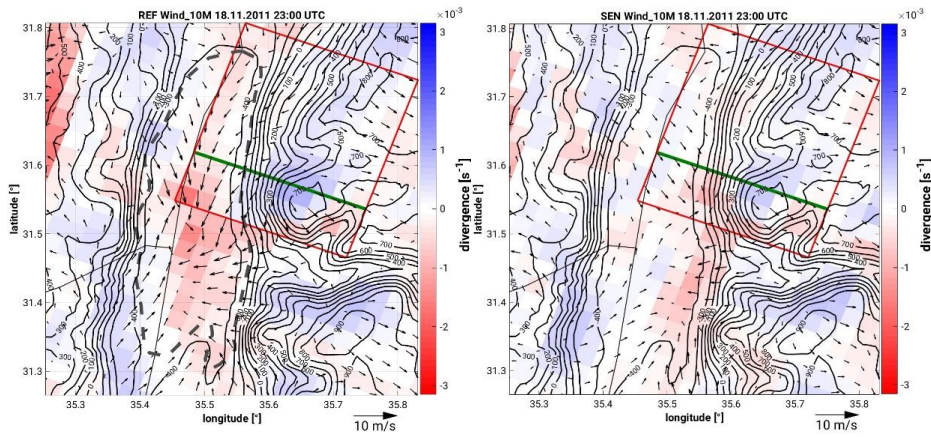

1142

1143   (b)

1144

1145

1146
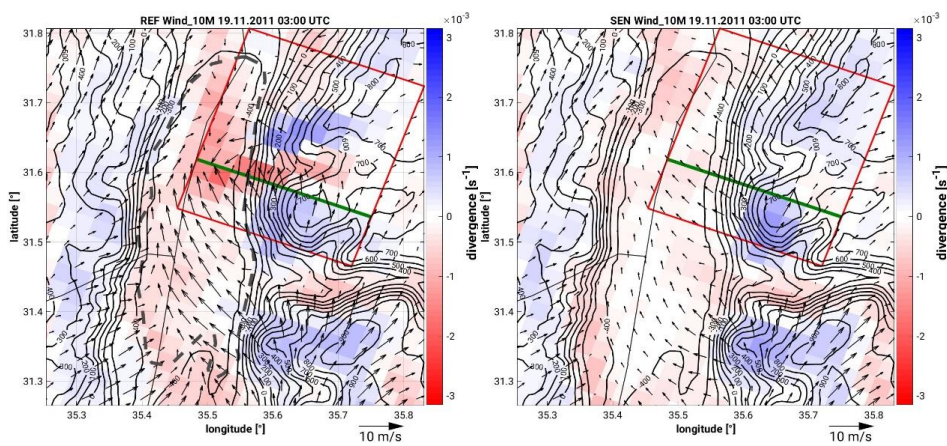
1147

1148

1149

1150

1151

1152

1153　　(c)

1154

1155

1156　　(d)

1157

1158

1159　Figure 10: Spatial distribution of 10-m horizontal wind (wind vectors; m/s) and
1160　corresponding divergence/convergence field (colour scale; s⁻¹) at 18 UTC, 20 UTC, 23
1161　UTC on the 19 November, and 03 UTC on the 20 November 2011 from the REF[19.11]
1162　(left) and SEN[19.11] (right) simulations. The topography is indicated by the black full
1163　isolines. The transects (B-C-D and B'-C'-D') corresponding to the locations in which
1164　temperature comparisons are made are indicated in Figure 10a. The green line
1165　indicates the position of the vertical cross-section in Figure 11.
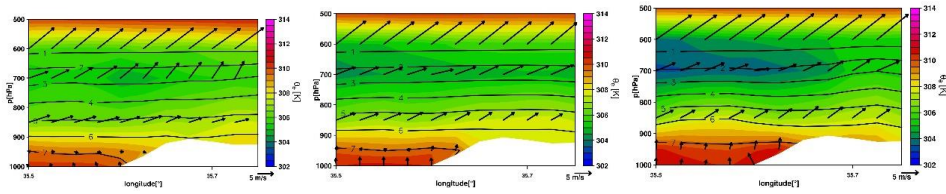
1166

1167

1168
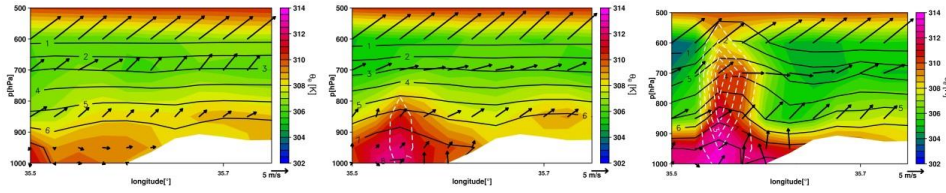
1169

1170

1171

1172

1173

1174 Figure 11: Vertical cross-section of equivalent potential temperature (colour scale; K),
1175 specific humidity (black isolines; g/kg), horizontal wind vectors (north-pointing upwards,
1176 m/s) and vertical velocity (white dashed contours with 1 m/s increments) of the REF[19.11]
1177 (top) and SEN[19.11] (bottom) simulations at 01 UTC (left), 02 UTC (middle) and 03 UTC
1178 (right). The location of the cross-section is indicated in Figure 10.

1179

1180

1181

1182

1183

1184

1185

1186

1187

1188

1189